

Constraints on Simplified Models for Dark Matter from LHC Dijet Searches

Sebastian Baum^{a,b} Riccardo Catena^c and Martin B. Krauss^{c,d}

^a*Oskar Klein Centre, Department of Physics, Stockholm University, AlbaNova, Stockholm SE-10691, Sweden*

^b*Nordita, KTH Royal Institute of Technology and Stockholm University, Roslagstullsbacken 23, 10691 Stockholm, Sweden*

^c*Chalmers University of Technology, Department of Physics, SE-412 96 Göteborg, Sweden*

^d*Dipartimento di Matematica e Fisica, Università di Roma Tre, Via della Vasca Navale 84, 00146 Rome, Italy*

E-mail: sbaum@fysik.su.se, catena@chalmers.se,
martin.krauss@chalmers.se

ABSTRACT: We present a reanalysis of the latest results from CMS dijet searches for an integrated luminosity of 36 fb^{-1} together with preliminary results for 78 fb^{-1} in the framework of simplified models for dark matter interacting with quarks through the exchange of a scalar, pseudoscalar, vector or pseudovector mediator particle. Within the same framework, we also project the sensitivity of dijet searches in future LHC runs and study how well the parameters of a simplified model could be reconstructed in case of a future discovery at the high luminosity (HL) LHC. Finally, we explore the possibility of discriminating different mediator scenarios by extending the sensitivity of dijet searches for simplified models through the use of angular information. It is the first time that these studies are performed systematically for the case of spin 0 mediators. Among other results we find: 1) no evidence for a dijet signal in the simplified model framework; 2) improvements due to an increased luminosity at the HL-LHC are significant, but mostly for heavy mediators, where dijet searches are limited by statistical, rather than systematical uncertainties; 3) Information on the angular separation of dijets could be used at the HL-LHC to discriminate different mediator scenarios.

Contents

1	Introduction	1
2	Theoretical Framework	3
3	Dijet Searches at the LHC	4
3.1	Background	5
3.2	Signal	5
4	Statistical Method	7
5	Exclusion Limits	8
6	Sensitivity Projections	13
7	Parameter Reconstruction	17
8	Conclusions	18
A	Signal fit and spectra	20

1 Introduction

In the quest for physics Beyond the Standard Model (BSM) at the Large Hadron Collider (LHC), *dijet* searches are a powerful probe of new particles coupling to quarks or gluons. Such searches generically focus on the resonant production of a new heavy particle in proton–proton collisions and the subsequent decay of the new particle into pairs of quarks, gluons, or a quark and a gluon. Due to hadronization, these quarks or gluons will then be seen in the detector as a pair of hadronic jets.

Neither the ATLAS nor the CMS collaboration has reported a significant excess to date, instead, they established upper limits on resonant dijet production cross sections. Currently, ATLAS has published results for generic (high-mass) dijet searches from 37 fb^{-1} of data taken during 2015 and 2016 [1], whereas CMS has presented results for 36 fb^{-1} of data from the 2016 dataset [2, 3], as well as preliminary results for 78 fb^{-1} from the combined 2016 and 2017 datasets [4]. More targeted analyses have been carried out beyond the generic (high-mass) dijet searches, for example focusing on low-mass resonances [5], or final states including *b-tagged* jets [6], additional charged leptons [7], or additional photons [8]. While such searches can make new regions of the parameter space available, we will focus on traditional dijet searches aimed at the multi-TeV mediator mass range in this work.

An interesting application of dijet searches is in the context of dark matter (DM). If the interaction between the visible and the dark sector is mediated by a new (heavy) particle,

this *mediator* can potentially be produced at the LHC and decay into a pair of quarks. While the DM particle is not directly involved in such processes, one can obtain valuable information about the underlying DM model. For example, the width and branching ratios (BRs) of the mediator depend on the properties of the DM candidate, which thus may be inferred in such an analysis. Focusing on the role of DM in dijet events, we study the interplay of dijet searches at the LHC and DM direct detection experiments in the simplified model framework in a companion paper [9].

Scenarios where the interaction between DM and the Standard Model (SM) is communicated by as yet undiscovered mediator particles are realized in many models of new physics, the most well-known being the various realizations of supersymmetry. For phenomenological purposes it often suffices to study *simplified models* which extend the SM’s particle content only by the DM candidate and the DM–SM mediator [10, 11]. Compared to the effective field theory (EFT) approach which has been widely used in the past to study classes of high-energy completions of the SM, the simplified model approach has the advantage that it remains valid when the momentum transfer in the process becomes of order of the mass of the mediator. This is particularly relevant for resonant dijet searches where one searches for the on-shell production of the mediator.

A list of simplified models for dark matter can be found in refs. [10–12]. Here, we will focus on simplified models with spin 0 or 1 mediators. Models with fermionic mediators do not give rise to resonant dijet signature and are thus not considered in this work. The ATLAS and CMS collaboration usually report limits in the simplified models framework for vector and axial-vector, i.e. spin 1, mediators only. Moreover, results are often reported for particular values of the coupling of mediators to DM particles, or correspondingly the width of the mediator, only. Reanalyses of the experimental data often allow for a range of values of the coupling to DM particles/the mediator’s width, but nonetheless focus mostly on spin 1 mediators, see e.g. refs. [13–20]. In this work, we obtain exclusion limits and future discovery projections for a wider class of mediators. In particular, we study the scalar, pseudoscalar, vector, and axial-vector mediator cases.

The remainder of this work is structured as follows: In section 2 we introduce the simplified model framework used in this analysis. In section 3 we describe dijet searches at the LHC in more detail. In section 3.1 we discuss the SM background for dijet searches, and in section 3.2 we discuss how we produce signal samples for the simplified models for our reanalysis of the LHC dijet searches. The statistical framework we use to set exclusion limits and sensitivity projections is described in section 4. In section 5 we present exclusion limits on the simplified models from the current dijet results reported by the LHC collaborations, before showing discovery prospects for dijet searches in future LHC runs in section 6. In section 7 we discuss how well the parameters of a simplified model could be reconstructed in case of a future discovery and point out how angular information of the dijet events could both be used to further improve the sensitivity of dijet searches and to distinguish between different dijet models in case of a discovery. We conclude in section 8.

2 Theoretical Framework

A list of simplified models for DM and their full Lagrangians can be found in Refs. [10–12]. The resonant dijet searches discussed here are sensitive to pairs of quarks produced via an s -channel resonance. Thus, we can restrict ourselves to simplified models containing mediators with spin $s_{\text{med}} = \{0, 1\}$. Fermionic mediators do not give rise to dijet final states via resonant processes and are thus not relevant for the searches discussed here. Further, dijet searches probe only the quark-quark-mediator vertex of the simplified model. While the DM-DM-mediator vertex is crucial for studying the DM phenomenology of the model and e.g. mono-jet signatures at the LHC, for dijet searches its only effect is that it alters the decay width of the mediator and the mediator’s branching ratios. In this work, we consider two benchmark cases. In the first, we assess the sensitivity of dijet searches on simplified models in the limit where all couplings between the mediator and the DM are set to zero. Then, the width of the mediator and its branching ratios are determined solely by the couplings between the SM and the mediator and we can set limits on these couplings. In the second case, we consider the width of the mediator as a free parameter, thus allowing for additional couplings of the mediator, e.g. to DM particles. Then, we can set limits on the dijet production cross section as a function of the mass and width of the mediator.

The relevant part of the Lagrangian of simplified models with $s_{\text{med}} = 0$ mediators is

$$\begin{aligned} \mathcal{L}_\phi \supset & \frac{1}{2} \partial_\mu \phi \partial^\mu \phi - \frac{m_\phi^2}{2} \phi^2 - \frac{\mu_1 m_\phi}{3} \phi^3 - \frac{\mu_2}{4} \phi^4 \\ & - h_1 \bar{q} q \phi - i h_2 \bar{q} \gamma_5 q \phi. \end{aligned} \quad (2.1)$$

Here, m_ϕ is the mass of the mediator ϕ and the μ_i are dimensionless self-couplings. Since the self-couplings of the mediators have no effect on the dijet signatures of the model, we set the $\mu_i = 0$ in the rest of this work. The couplings of ϕ to quarks h_i should in general be understood as (6×6) matrices and the quark fields q as vectors in flavor space, $q = (u, d, c, s, t, b)$. In this work, we will assume flavor-diagonal and universal quark couplings such that the h_i can be understood as numbers instead of matrices. We will study the cases where only one of the (universal) h_i is different from zero at a time: in the following we refer to the $h_1 \neq 0$ case as a *scalar* mediator and the $h_2 \neq 0$ case as a *pseudoscalar* mediator.

Similarly, the relevant part of the Lagrangian for simplified models with $s_{\text{med}} = 1$ mediators is

$$\begin{aligned} \mathcal{L}_G \supset & -\frac{1}{4} \mathcal{G}_{\mu\nu} \mathcal{G}^{\mu\nu} + \frac{m_G^2}{2} G_\mu G^\mu \\ & - h_3 \bar{q} \gamma_\mu q G^\mu - h_4 \bar{q} \gamma_\mu \gamma_5 q G^\mu, \end{aligned} \quad (2.2)$$

where $\mathcal{G}^{\mu\nu}$ is the field-strength tensor of the mediator G^μ , m_G its mass, and the h_i are the dimensionless couplings of G^μ to quarks. As in the $s_{\text{med}} = 0$ case the h_i in general should be understood as (6×6) matrices, but can be understood as numbers for the purposes of this work because we consider universal and flavor-diagonal quark couplings. We will only consider one of the h_i different from zero at a time; the $h_3 \neq 0$ case is referred to as the *vector* mediator case, and the $h_4 \neq 0$ case as *axial-vector* in the following.

When not talking about a specific model, we will use m_{med} (Γ_{med}) to refer to the mass (width) of the respective mediator, and g_q to refer to the quark-mediator coupling different from zero. Depending on our assumptions on the width of the mediator, we thus obtain models specified by two or three parameters. In the case where we assume the mediator to couple only to quarks, the model is specified by the parameters $\{m_{\text{med}}, g_q\}$, and the width Γ_{med} is a function of m_{med} and g_q only. In the case where we treat the width as a free parameter to include the possibility that the mediator decays into particles other than quarks, the model is specified by the parameters $\{m_{\text{med}}, g_q, \Gamma_{\text{med}}\}$.

The latter case includes in particular the region of parameter space where the mediator has a sizeable branching into pairs of DM candidates. Note though, that the larger the branching ratio into pairs of DM particles is, the less sensitive dijet searches are. This is because for fixed values of m_{med} and g_q , the dijet production cross section scales as $[\sigma \propto (\Gamma_{qq}/\Gamma_{\text{med}})^2]$, where Γ_{qq} is the partial width of the mediator into quark pairs, and $(\Gamma_{\text{med}} = \Gamma_{qq} + \Gamma_{\text{DM}} + \dots)$, where Γ_{DM} is the partial width into pairs of DM particles and the “...” indicate the partial width corresponding to any additional decay channels of the mediator. The broadening of the resonant dijet spectrum with increasing decay width further depreciates the sensitivity of dijet searches towards such models: the wider the resonance is, the more challenging it is to differentiate the dijet spectrum from resonant production of the mediator from the smoothly falling SM background discussed in the following sections.

3 Dijet Searches at the LHC

Dijet searches are performed by both the ATLAS and the CMS collaborations. As of yet, the collaborations have not reported observations of statistically significant excesses and instead set upper limits on resonant dijet processes. Typically, such results are presented in a model independent fashion as upper limits on the dijet production cross section as a function of mediator mass. In addition, the experimental collaborations often reported results in the simplified model framework, setting constraints on the mediator-quark-quark coupling g_q as a function of mediator mass. However, such results are presented for spin 1 (vector and axial-vector) mediators only, and usually only for particular values of the mediators width. In this work, we present exclusion limits from current LHC data and projections for future LHC runs for spin 1 as well as for spin 0 (scalar and pseudoscalar) mediators and for a range of mediator widths.

CMS defines a low mass region from 0.6 TeV to 1.6 TeV and a separate region for resonances above 1.6 TeV [2, 3] for dijet searches. We will focus on the high-mass region in this study and use the latest published results corresponding to 36 fb^{-1} of data at $\sqrt{s} = 13 \text{ TeV}$ [2, 3] as well as preliminary results for 78 fb^{-1} of data [4]. For our analysis, we simulate signal events as well as SM background samples as described further below. We use cuts similar to those employed in the CMS searches, cf. refs. [2, 3]: We use anti- k_T jets [21, 22] with a distance parameter of $\Delta R = 0.4$. Only jets with transverse momentum $p_T > 30 \text{ GeV}$ and pseudo-rapidity $|\eta| < 2.5$ are considered in the analysis. Further, the two jets with largest p_T in the event (the *leading jets*) are used as seeds for the construction of

so-called *widejets* by merging all jets within $\Delta R = \sqrt{(\Delta\eta)^2 + (\Delta\phi)^2} < 1.1$ of the leading jets with the seed jets. In order to suppress t -channel background events, the resulting widejets must be separated in pseudorapidity by less than $|\Delta\eta_{jj}| < 1.3$. The CMS analyses further make a number of quality cuts on the reconstructed jets. In our analysis, we only require that less than 90% of each of the two leading jets' respective energies are deposited in the electromagnetic calorimeter.

Note that the ATLAS collaboration uses somewhat different selection cuts in their analysis, e.g. they require $p_T > 400$ GeV for the leading jet [1]. However, we expect the differences in the selection cuts between the ATLAS and CMS analyses to only have minor impact on the reported limits and projected sensitivity. Thus, results found in this work are expected to apply to both the ATLAS and CMS collaborations' results despite us using CMS-like cuts.

3.1 Background

The dominant background source for dijet searches at the LHC are ($pp \rightarrow qq/qg/gg + X$) SM processes, where p is a proton, q a quark, g a gluon, and X indicates additional SM particles. In their analysis, both ATLAS and CMS use data-driven methods to estimate the SM background. The collaborations fit the measured background spectra by [1–4]

$$\frac{d\sigma}{dm_{jj}} = p_0 \frac{(1-x)^{p_1}}{x^{p_2+p_3 \log(x)}} , \quad (3.1)$$

where $x \equiv m_{jj}/\sqrt{s}$ with m_{jj} the invariant mass of the (wide)jets and \sqrt{s} the proton-proton center of mass energy, and the p_i are the fit parameters. We use the same fit-function as given in eq. (3.1) which we fit to data from the CMS collaboration to obtain the p_i . We show the CMS dijet data for 36 fb^{-1} [2, 3] together with the fitted background parameterization in the left panel of fig. 1. A similar plot for 78 fb^{-1} can be found in [4]. Note that this parameterization of the background allows us to predict the background for larger luminosities without the need to carry out dedicated collider simulations of the SM dijet background.

In order to perform an independent test of the background parameterization and in particular to obtain double-differential distributions $d^2\sigma/dm_{jj}d\Delta\eta_{jj}$ we will make use of in section 6, we have performed our own SM background simulations using `MadGraph5` [23] for the simulation of the ($pp \rightarrow qq/qg/gg + X$) events, `pythia8` [24, 25] for showering, and `Delphes3` [26] for fast detector simulation using the cuts described above.

3.2 Signal

In order to obtain limits from current dijet searches and to make projections for future searches we need both the SM background spectra and the signal spectra in the respective simplified model cases we consider. For our main analysis, we first simulate all possible signal processes

$$pp \rightarrow \text{Mediator} \rightarrow \bar{q}q + X , \quad (3.2)$$

for each of the simplified model cases considered here {(pseudo)scalar, (axial-)vector} over a grid of model parameters m_{med} , g_q (and Γ_{med} when treating the width as an independent

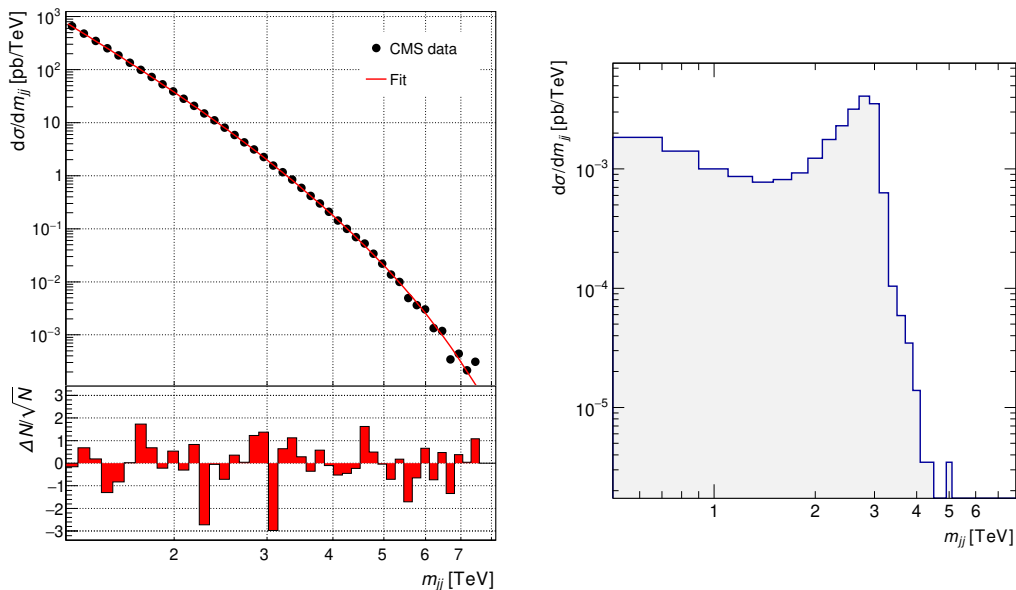


Figure 1: *Left:* Invariant dijet mass spectrum measured by CMS for the 36 fb^{-1} [2, 3] dataset obtained from the `hepdata` server [27]. In the upper panel, the black dots show the CMS data and the red line shows the background parameterization in eq. (3.1) after fitting. The lower panel shows the residuals of the data with respect to the fitted background parameterization divided by the statistical error of the data. *Right:* Dijet mass spectrum of the simulated signal for a vector mediator with $\{m_{\text{med}} = 3.0 \text{ TeV}, g_q = 0.1\}$ under the assumption that Γ_{med} is determined by decays into quarks only. The bin width is set to 25 GeV. Note that the scale of the axes differs between the panels.

parameter) with `WHIZARD` [28, 29].¹ In eq. (3.2), X stands for additional SM particles. For example, when simulating $pp \rightarrow \text{Mediator} \rightarrow \bar{t}t$ events we also simulate the ($t \rightarrow Wb$) decays and the subsequent decays of the W -bosons into pairs of SM particles in `WHIZARD`. Note, that no b -jet veto is employed in the dijet analyses considered here. Parton distribution functions are implemented via the `CT14lo` set as obtained from `LHAPDF6` [31]. For showering and hadronization we use `pythia8`. For the (fast) detector simulation we use `Delphes3` with `FASTJET` [32] for jet reconstruction and the default CMS configuration file except that we modified the jet-reconstruction parameters to match those employed in the CMS analyses. We use our own C++ code together with several `ROOT` [33] libraries to analyze the signal, including the application of selection cuts, widejet reconstruction, and signal fitting.

We have validated our tool-chain for event generation and analysis with an independent simulation chain using `MadGraph5` for the generation of the hard event, `pythia8` for showering and `Delphes3` for fast detector simulation.

We show an example of a signal spectrum for the vector mediator model for $\{m_{\text{med}} = 3.0 \text{ TeV}, g_q = 0.1\}$ in the right panel of fig. 1. Here, we assume that the mediator couples only to quarks, thus, its width is determined by m_{med} and g_q . The tail of the signal

¹We use implementations of the simplified models for `WHIZARD` developed in ref. [30].

at low invariant masses of the widejet system $m_{jj} \ll m_{\text{med}}$ arises from showering and hadronization.

The signal spectra can be fit by

$$\frac{d\sigma}{dm_{jj}} = p_0 V(m_{jj} - p_2, p_3, p_1) e^{p_4 \frac{m_{jj}}{p_2}} \left(\frac{m_{jj}}{p_2} \right)^{p_5}, \quad (3.3)$$

where the p_i are fit parameters. The parameter p_0 has dimensions of mass^{-3} , $\{p_1, p_2, p_3\}$ have dimension of mass, and $\{p_4, p_5\}$ are dimensionless.

$$V(x, \sigma, \gamma) = \int_{-\infty}^{\infty} \frac{1}{\sqrt{2\pi}\sigma} e^{-\frac{x'^2}{2\sigma^2}} \frac{\gamma}{[(x-x')^2 + \gamma^2]} dx', \quad (3.4)$$

is a Voigt profile, the convolution of a Lorentzian profile with a Gaussian. Here, the Lorentzian profile accounts for the shape of the resonance, while the Gaussian profile accounts for the broadening due to the finite detector resolution. Out of the parameters, p_1 is related to the mediator's width, p_2 to its mass, and p_3 reflects the invariant mass resolution of the detector. p_0 controls the overall normalization of the differential cross section. The parameters p_4 and p_5 control the exponential and power-law tails of the differential cross section. They are purely phenomenologically motivated and account for the low energy tail of the spectrum.

In fig. 8, located in the appendix, we show simulated signal spectra with the respective fits for several parameter points. The parameterization of the signal spectra in eq. (3.3) suffices to fit the signal well for the wide range of parameters $\{m_{\text{med}}, g_q\}$ shown in fig. 8.

In appendix. A we list the fit parameters for several models and parameter points, which can be used for further analyses without the need for a full simulation. In the following analyses, we use the simulated signal spectra, scaled to the appropriate luminosity, and not the parametric fits to these signal spectra.

4 Statistical Method

We compute exclusion limits and sensitivity projections using the profile likelihood method. Our analysis is similar to the one carried out by the CMS collaboration, and follows the procedure outlined in ref. [34]. Computing exclusion limits, we test the background plus signal hypothesis, H_1 , against the background only hypothesis, H_0 , and compute the significance with which a point in parameter space can be excluded. When projecting the sensitivity of dijet searches in future LHC runs, we test the null hypothesis H_0 against the alternative H_1 and compute the significance with which a point in parameter space can be observed.

The significance,

$$Z = \Phi^{-1}(1 - p) \quad (4.1)$$

is related to the p -value via the quantile Φ^{-1} of a Gaussian distribution with mean 0 and variance 1. For example, the usual 95% confidence level (C.L.) with p -value 0.05 corresponds to $Z = 1.64$. In general, the significance is computed from the likelihood function \mathcal{L} for finding a given signal $\mathbf{s} = \{s_1, \dots, s_N\}$ over a background $\mathbf{b} = \{b_1, \dots, b_N\}$

for a dataset $\mathbf{n} = (n_1, \dots, n_N)$, where N is the number of considered bins in the dijet invariant mass,

$$\mathcal{L}(\mathbf{s}, \boldsymbol{\theta}) = \prod_{i=1}^N \frac{(s_i + b_i(\boldsymbol{\theta}))^{n_i}}{n_i!} e^{-[s_i + b_i(\boldsymbol{\theta})]}, \quad (4.2)$$

and $\boldsymbol{\theta}$ is an array of nuisance parameters, which in our case correspond to the background fit parameters from eq. (3.1). In order to calculate the significance from the likelihood, we construct a profile likelihood ratio, λ . The exact form of λ depends on whether we calculate the significance for exclusion limits or sensitivity projections. For exclusion limits, we use the profile likelihood ratio

$$\lambda = \frac{\mathcal{L}(\mathbf{s}, \widehat{\boldsymbol{\theta}})}{\mathcal{L}(\mathbf{0}, \widehat{\boldsymbol{\theta}})}, \quad (4.3)$$

where $\widehat{\boldsymbol{\theta}}$ and $\widehat{\boldsymbol{\theta}}$ are the nuisance parameters that maximize the likelihood function \mathcal{L} for the signals \mathbf{s} and $\mathbf{0}$, respectively. Similarly, for sensitivity projections we use the profile likelihood ratio

$$\lambda = \frac{\mathcal{L}(\mathbf{0}, \widehat{\boldsymbol{\theta}})}{\mathcal{L}(\mathbf{s}, \widehat{\boldsymbol{\theta}})}. \quad (4.4)$$

In both cases, from the profile likelihood ratio we construct the test statistic $q = -2 \ln \lambda$, from which we obtain [34]

$$Z \simeq \sqrt{q}. \quad (4.5)$$

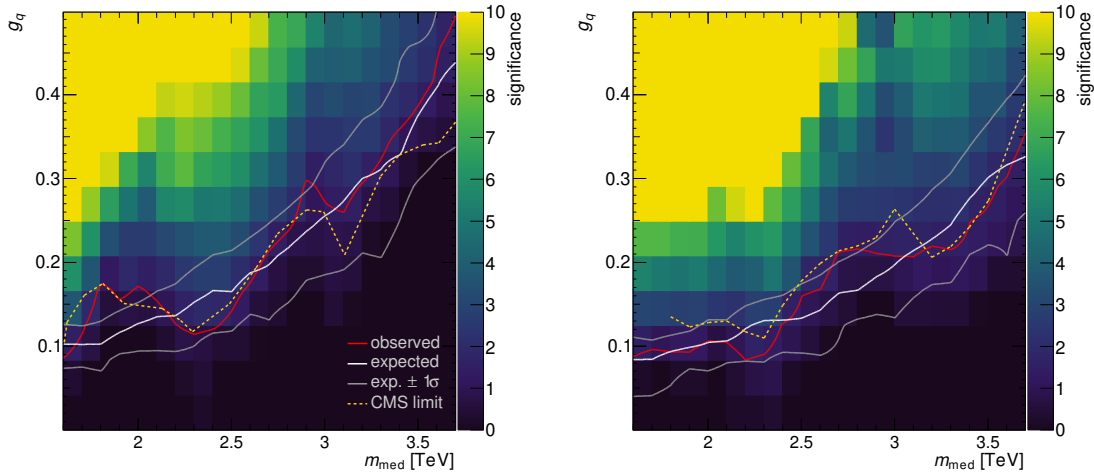
In our analysis, we are interested in *observed* exclusion limits and *expected* exclusion limits. In the former case, we compute the significance using $n_i = n_i^{\text{CMS}}$, where n_i^{CMS} is the number of observed dijet events at CMS in the i -th dijet mass bin.² In the latter case, we assume $n_i = b_i(\boldsymbol{\theta}_{\text{bf}})$, where $\boldsymbol{\theta}_{\text{bf}}$ is the value of $\boldsymbol{\theta}$ that maximises $\mathcal{L}(\mathbf{0}, \boldsymbol{\theta})$ for $n_i = n_i^{\text{CMS}}$. As already anticipated, we are also interested in computing the significance for sensitivity projections. In this case, we use the dataset $n_i = b_i(\boldsymbol{\theta}_{\text{bf}}) + s_i$. In all cases discussed above, when maximizing the likelihood with respect to $\boldsymbol{\theta}$ to obtain $\widehat{\boldsymbol{\theta}}$ or $\widehat{\boldsymbol{\theta}}$ at a given point in parameter space, we exclude a window around the mediator mass in the dijet invariant mass spectrum³.

5 Exclusion Limits

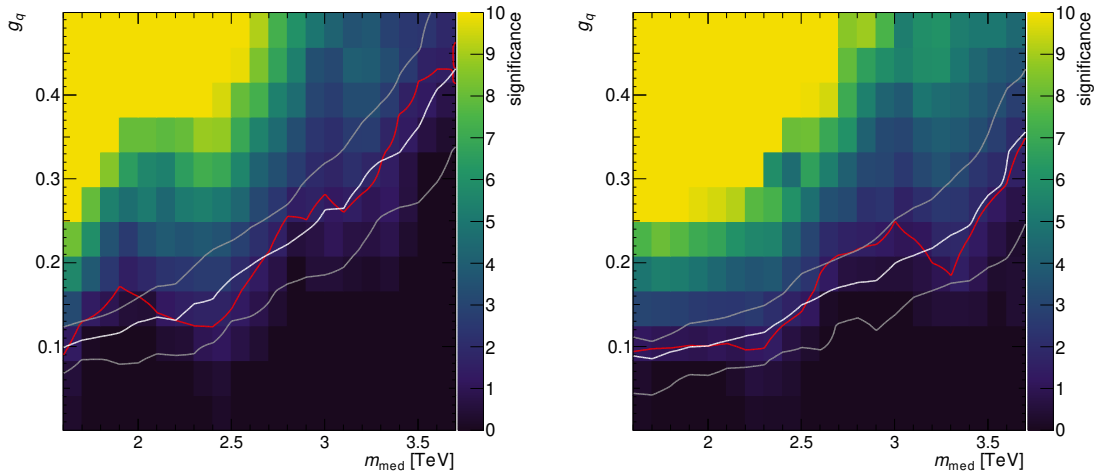
In this section we present exclusion limits for the (pseudo)scalar and (axial-)vector mediator cases from the 36 fb^{-1} [2, 3] and 78 fb^{-1} [4] CMS data. We obtain 95% C.L. exclusion limits by simulating signals for each parameter point for a grid in $\{m_{\text{med}}, g_q\}$ ($\{m_{\text{med}}, g_q, \Gamma_{\text{med}}\}$) space as described in section 3.2 and computing the profile likelihood for the null hypothesis according to the procedure outlined in section 4.

²When setting limits based on the CMS result from 36 fb^{-1} of data, n_i^{CMS} is the measured dijet spectrum obtained from [27]. For limits based on 78 fb^{-1} , n_i^{CMS} is taken from [4].

³The masked region is defined by excluding the region bounded by the bins with largest and smallest invariant mass in which the profile likelihood ratio λ , defined in eq. (4.3), takes values $\lambda > 1$.



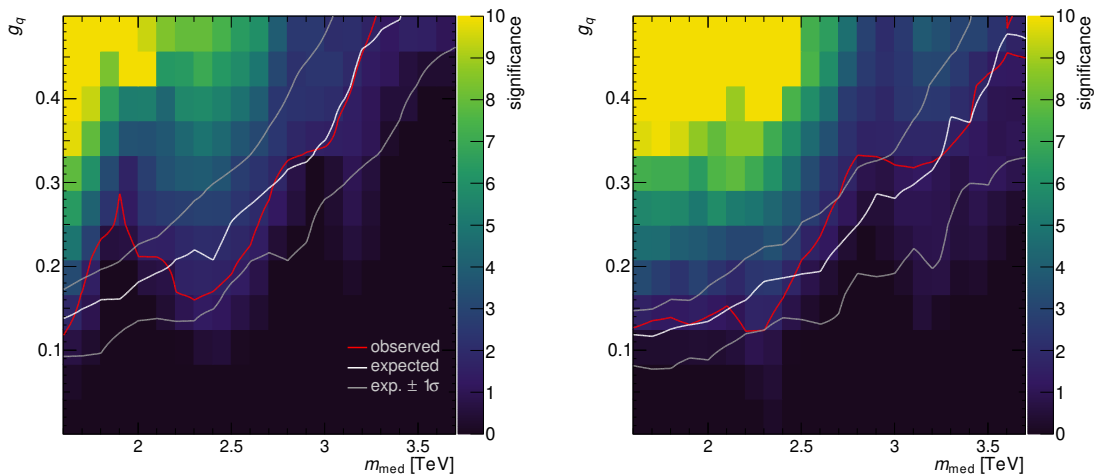
(a) Vector Mediator ($h_3 \neq 0$)



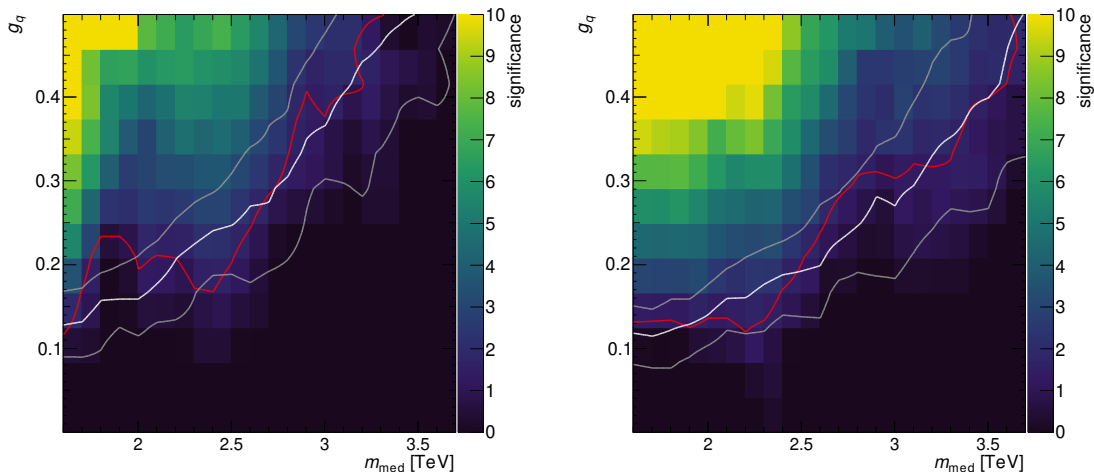
(b) Axial-Vector Mediator ($h_4 \neq 0$)

Figure 2: Exclusion limits for the vector mediator (upper panels) and axial-vector mediator (lower panels) under the assumptions that the mediator couples to quarks only. The left panels are for the 36 fb^{-1} CMS data [2, 3] while the right panels are for the 78 fb^{-1} data [4]. The color scales show the significance [defined in eq. (4.1)] for which a parameter point in the $m_{\text{med}} - g_q$ plane could be excluded. The white line shows the expected 95% C.L. exclusion limit with the gray lines indicating the 1σ error bands around the expected limit. The red line shows the 95% C.L. exclusion limit obtained from the observed data. For comparison, in the upper panels we show the 95% C.L. exclusion limit reported by the CMS collaboration for the vector mediator case with the dashed yellow line.

We show our results for the vector and axial-vector mediator cases in fig. 2 and for the scalar and pseudoscalar cases in fig. 3 under the assumption that the mediator couples



(a) Scalar Mediator ($h_1 \neq 0$)



(b) Pseudoscalar Mediator ($h_2 \neq 0$)

Figure 3: Same as fig. 2 but for the scalar mediator (upper panels) and pseudoscalar mediator (lower panels) cases.

to quarks only, thus its width Γ_{med} is a function of m_{med} and g_q only. In these figures, we show both the expected and observed limits as well as the significance [as defined in eq. (4.1)] for which a parameter point in the $m_{\text{med}} - g_q$ plane is excluded by the CMS data. For comparison, we also show the limit obtained by the CMS collaboration for the vector mediator case.

We begin by discussing our results for the vector mediator case, shown in the upper panels of fig. 2. For both the 36 fb^{-1} and the 78 fb^{-1} data, the limits we obtain are within $\sim 1 \sigma$ of the respective expected limits, indicating that both CMS datasets are compatible with the background-only hypothesis and show no evidence for a dijet signal from a simplified

model with a vector mediator. For the 36 fb^{-1} , the largest deviations from the expected limits are for mediator masses of $\sim 2 \text{ TeV}$ and $\sim 3 \text{ TeV}$ where the observed limits are $\sim 1.5 \sigma$ and $\sim 1 \sigma$ weaker, respectively, than the expected limit. Although of small statistical significance, these excesses can be understood from the correlated residuals in the CMS data with respect to the background fit at the corresponding invariant masses, cf. the left panel of fig. 1. Our limits are in good agreement with those obtained by the CMS collaboration for vector mediator from the same dataset. Note that while both the CMS collaboration and we employ similar statistical techniques, our analysis is independent from those carried out by the CMS collaboration. The only common input are the measured dijet spectra.

Considering the results from the 36 fb^{-1} data we find the strongest limits for the smallest mediator masses considered, excluding (universal) couplings of the mediator to quarks larger than $g_q \sim 0.1$ for mediator masses $m_{\text{med}} \sim 1.6 \text{ TeV}$ at 95 % C.L. With increasing mediator mass the limits weaken. This is because the background spectrum (signal spectrum) is falling steeply with m_{jj} (m_{med}). The limits are driven mostly by the data in the bins of the invariant mass spectrum comparable to m_{med} . Thus, with increasing mediator mass the relative statistical uncertainty in the relevant part of the dijet spectrum is increasing, leading to weaker exclusion limits. For mediator masses $m_{\text{med}} \sim 3.5 \text{ TeV}$ we exclude couplings to quarks $g_q \gtrsim 0.4$.

Comparing the results from the 36 fb^{-1} data to those from the 78 fb^{-1} data, we find that the larger luminosity allows for more stringent exclusion limits, in particular for larger mediator masses. Recall that the exclusion limits are driven by the portion of the observed data where the invariant mass of the widejet system m_{jj} approximately corresponds to the mass of the mediator. The SM background spectrum is monotonically falling with m_{jj} . For the smallest mediator masses considered here of $m_{\text{med}} \sim 1.6 \text{ TeV}$, the relevant portion of the dijet spectrum is already dominated by systematic errors, thus, without changing the analysis techniques no improvements in the limits are expected by increasing the luminosity. For heavier mediators on the other hand, the obtained exclusion limits are limited by the statistical error of the relevant portion of observed dijet spectra, thus, we find sizable differences in the observed limits between the 36 fb^{-1} and the 78 fb^{-1} datasets. For mediator masses of $m_{\text{med}} \sim 2 \text{ TeV}$, the 95 % C.L. exclusion limits strengthen from $g_q \lesssim 0.15$ from the 36 fb^{-1} dataset to $g_q \lesssim 0.10$ from the 78 fb^{-1} dataset. For heavier vector mediators $m_{\text{med}} \sim 3.5 \text{ TeV}$ we find that the limits strengthen from $g_q \lesssim 0.4$ to $g_q \lesssim 0.25$.

For the axial-vector case, cf. the lower panels of fig. 2, we find results very similar to the vector mediator case. This is because the limits are driven by decays of the mediator into the lighter quark flavors $q = \{u, d, c, s, b\}$. In the limit of vanishing quark masses the dijet cross sections for vector and axial-vector mediator become equal.

Considering (pseudo)scalar mediators, cf. fig. 3, we again find almost identical limits when comparing the scalar and the pseudoscalar cases. As in the case of vector and axial-vector mediators, this is because the dijet production cross sections for scalar and pseudoscalar mediators become equal in the limit of massless quarks. Comparing the limits for (pseudo)scalar mediators to the (axial-)vector case, we find that while the limits on the coupling to quarks are similar for mediator masses $m_{\text{med}} \sim 1.6 \text{ TeV}$, the limits for the

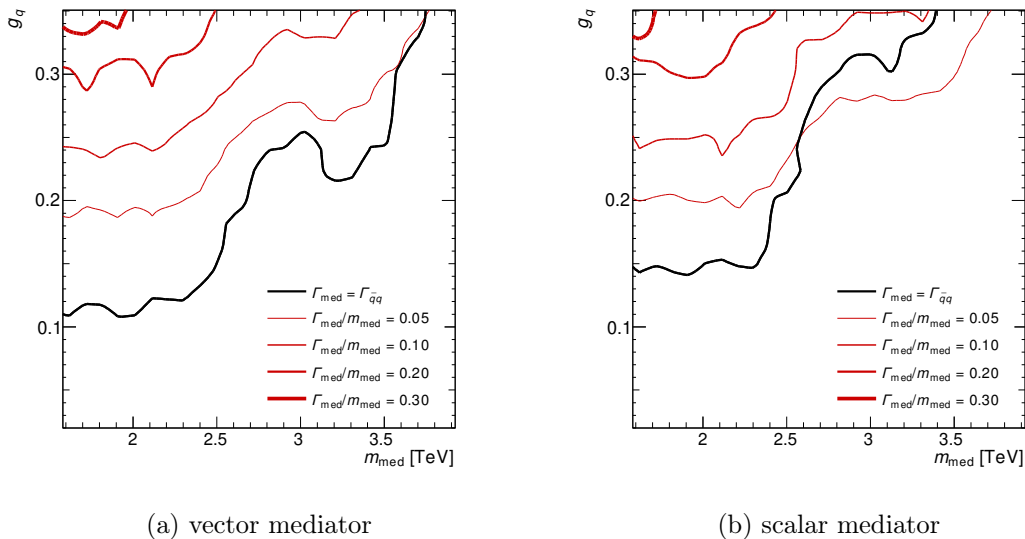


Figure 4: 95 % C.L. exclusion limits for the vector mediator (left panel) and scalar mediator (right panel) cases from the 78 fb^{-1} data. In fig. 2 and fig. 3 we showed exclusion limits under the assumption that the mediator couples to quarks only and thus the mediator’s width Γ_{med} is a function of its mass m_{med} and the coupling to quarks g_q only. Here, we treat Γ_{med} as a free parameter accounting for additional decay channels of the mediator, for example into pairs of DM candidate particles. The different lines are for different values of Γ_{med} as indicated in the legend. The axial-vector and pseudoscalar cases not shown here would look very similar to the vector and scalar cases, respectively.

(pseudo)scalar cases are considerably weaker for heavier mediators. For mediator masses of $m_{\text{med}} \sim 3.5 \text{ TeV}$ couplings of the mediator to quarks larger than $g_q \sim 0.55$ are excluded for (pseudo)scalar mediators from the 36 fb^{-1} dataset, while for (axial-)vector mediators the data constrained $g_q \lesssim 0.4$ for such mediator masses. The 78 fb^{-1} dataset excludes couplings larger than $g_q \sim 0.4$ for (pseudo)scalar mediators with $m_{\text{med}} \sim 3.5 \text{ TeV}$ while for (axial-)vector mediators the same data constrained the couplings to $g_q \lesssim 0.25$.

The results shown in fig. 2 and fig. 3 assume that the mediator decays only into quarks, thus, its width Γ_{med} is a function of its mass m_{med} and the coupling to quarks g_q only. In fig. 4 we show 95 % C.L. exclusion limits for the vector and scalar mediator case treating Γ_{med} as a free parameter to account for additional decay channels of the mediator. In particular, such decay channels may include decays of the mediator into pairs of DM candidate particles. We do not show results for the axial-vector and pseudoscalar cases, since the limits would be very similar to the vector and scalar cases, respectively, cf. the discussion above.

Increasing the width of the mediator with respect to the width given by the decay into quarks only weakens the limits via two effects: 1) Increasing the width results in a broader signal spectrum which is more difficult to distinguish from the smooth SM background. 2) Increasing the width reduces the overall dijet production cross section for the signal,

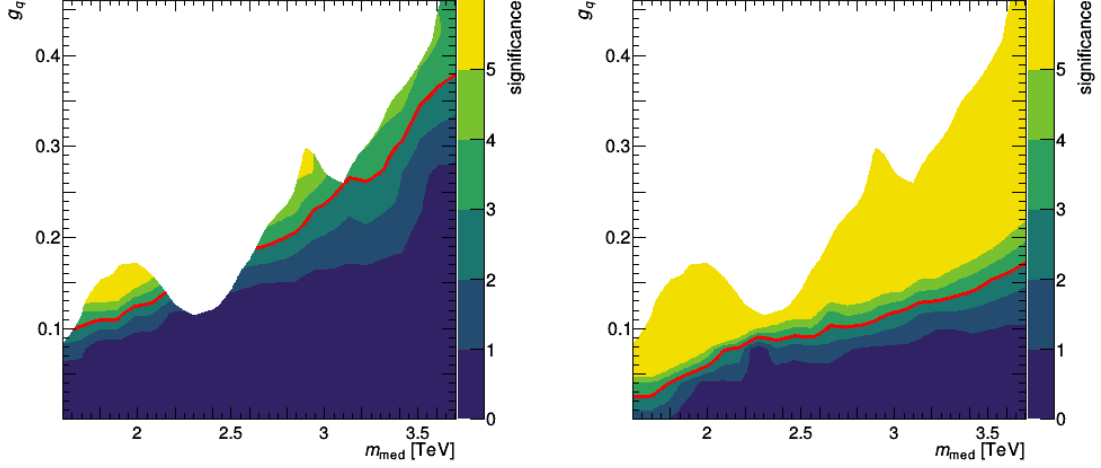
since $[\sigma \propto (\Gamma_{qq}/\Gamma_{\text{med}})^2]$ in the narrow width approximation. Here, Γ_{qq} is the partial width into pairs of quarks fixed by the mediator’s mass and the coupling to quarks, and ($\Gamma_{\text{med}} = \Gamma_{qq} + \dots$), with “ \dots ” indicating the partial width into additional decay channels, is the width of the mediator.

In the limit of massless quarks and for a scalar mediator we can use the approximation $\Gamma_{qq}/m_{\text{med}} \sim 18h_1^2/8\pi$, where the factor of 18 accounts for the summation over all possible flavor and color states. For a vector mediator we obtain $\Gamma_{qq}/m_{\text{med}} \sim (2/3) \times 18h_3^2/8\pi$, where the additional factor of $2/3$ comes from averaging over the polarization states of the vector mediator. The same approximations would apply for a pseudoscalar and an axial-vector, respectively, since their decay width into quarks differs only for non-zero quark masses. The exact formula for Γ_{qq} for all mediators discussed here can be found in ref. [35]. For a vector mediator we obtain then, for instance, $[\Gamma_{qq}/m_{\text{med}}(g_q = h_3 = 0.1) = 0.005]$ and $[\Gamma_{qq}/m_{\text{med}}(0.3) = 0.04]$, while for a scalar mediator we have $[\Gamma_{qq}/m_{\text{med}}(g_q = h_1 = 0.1) = 0.007]$ and $[\Gamma_{qq}/m_{\text{med}}(0.3) = 0.06]$. Thus, we can understand the results shown in in fig. 4: In the case of a vector mediator, the limit assuming decay into quarks only is stronger than the limit for $\Gamma_{qq}/m_{\text{med}} = 0.05$ for the entire range of mediator masses shown. For a scalar mediator, instead, the limits in the $\Gamma_{\text{med}} = \Gamma_{qq}$ case exclude quark couplings $g_q \gtrsim 0.25$ for mediator masses $m_{\text{med}} \sim 2.7 \text{ TeV}$ and even larger g_q for larger m_{med} . The partial width into quarks Γ_{qq} is larger than $\Gamma_{qq}/m_{\text{med}} = 0.05$ for $g_q \gtrsim 0.25$. Thus, for the $\Gamma_{\text{med}}/m_{\text{med}} = 0.05$ case we exclude couplings g_q smaller than for the $\Gamma_{\text{med}} = \Gamma_{qq}$ case for $m_{\text{med}} \gtrsim 2.7 \text{ TeV}$, although it should be noted that limits for $\Gamma_{\text{med}} < \Gamma_{qq}$ are of course purely hypothetical and do not correspond to a physical scenario.

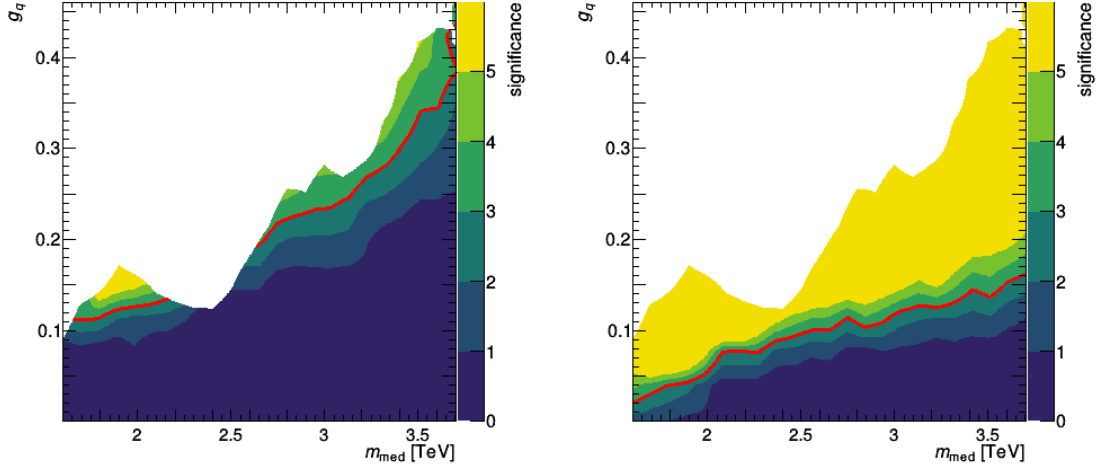
6 Sensitivity Projections

Assuming that the selection cuts will remain unchanged with respect to those employed in the current dijet analyses, we can project the sensitivity of dijet searches in future LHC runs without the need to run dedicated SM background simulations. To this end, we use the background fit to the 36 fb^{-1} CMS dataset described in section 3.1 and rescale the background to the appropriate luminosity. Here, we consider two benchmark cases: an integrated luminosity of 300 fb^{-1} as expected to be collected at the end of Run 3 of the LHC in 2023, and an integrated luminosity of 3000 fb^{-1} as expected to be collected by ~ 2037 after the high luminosity (HL) upgrade of the LHC. Using the fit of the background spectrum to the existing 36 fb^{-1} dataset entails that our projections do not account for improvements in sensitivity from a possible increase of the LHC’s center of mass energy from the current $\sqrt{s} = 13 \text{ TeV}$ to $\sqrt{s} = 14 \text{ TeV}$. However, the impact of such a modest increase in \sqrt{s} on the projected sensitivity would be much smaller than from the increase in luminosity by a factor of $10 - 100$ with respect to 36 fb^{-1} of data. Together with our simulated signal samples, we can project the future sensitivities using the statistical procedure outlined in section 4.

We show sensitivity projections for the vector and axial-vector cases in fig. 5 and for the scalar and pseudoscalar cases in fig. 6 under the assumption that the mediator couples to quarks only, thus, its width is a function of m_{med} and g_q only. The improvements with



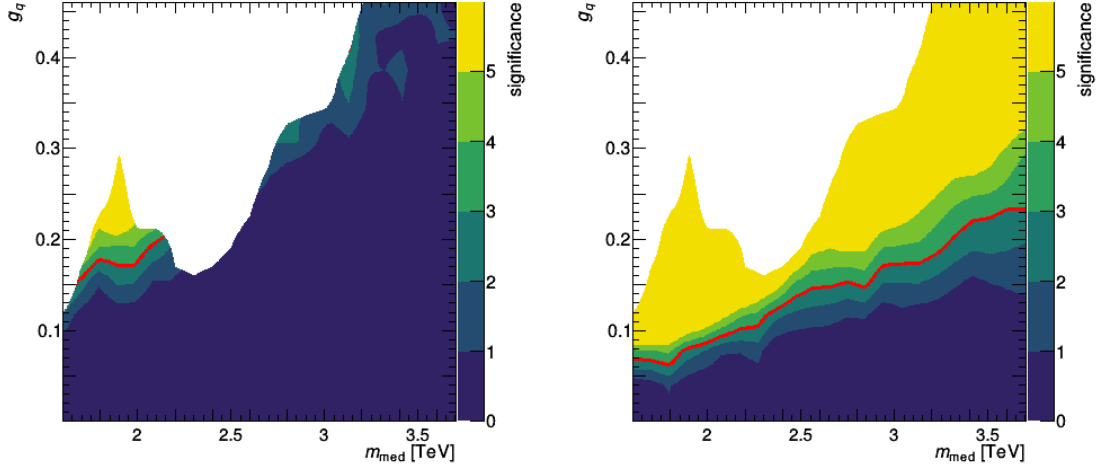
(a) Vector Mediator ($h_3 \neq 0$)



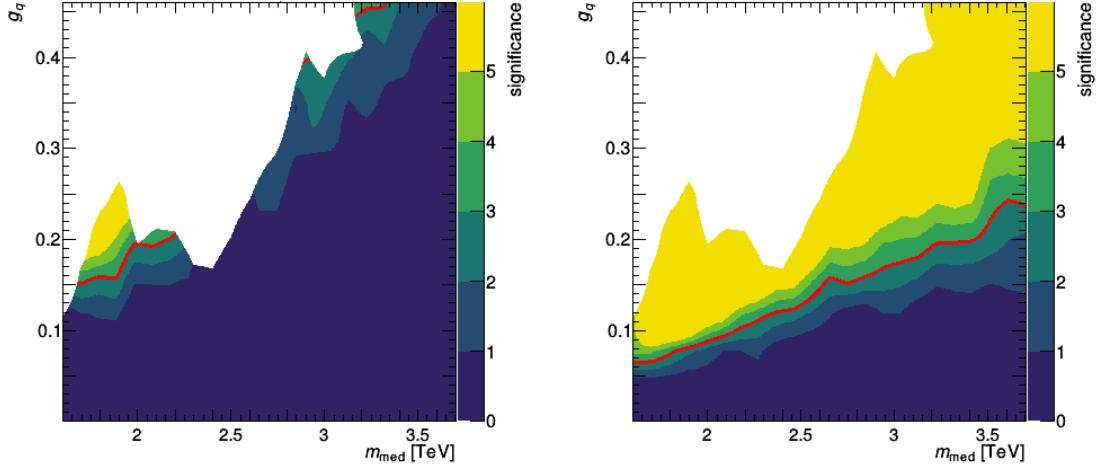
(b) Axial-Vector Mediator ($h_4 \neq 0$)

Figure 5: Sensitivity projections for the vector mediator (upper panels) and axial-vector mediator (lower panels) in future LHC runs under the assumption that the width of the mediator is determined by decays into quarks only. The left panels are for 300 fb^{-1} of data expected to be collected after Run 3 of the LHC. The right panels are for 3000 fb^{-1} of data as expected to be collected by the High Luminosity (HL) upgrade of the LHC. The color scale shows the significance [defined in eq. (4.1)] with which a parameter point in the $m_{\text{med}} - g_q$ parameter plane could be observed. The red line corresponds to the contour with a statistical significance of 3σ for the discovery of a dijet signal. The white region is the parameter space excluded by the 36 fb^{-1} data, cf. fig. 2.

respect to the currently excluded region of parameter space is rather similar for all cases considered here. As discussed in section 5, for the smallest mediator masses $m_{\text{med}} \sim 1.6 \text{ TeV}$



(a) Scalar Mediator ($h_1 \neq 0$)



(b) Pseudoscalar Mediator ($h_2 \neq 0$)

Figure 6: Same as fig. 5 but for the scalar (upper panel) and the pseudoscalar (lower panel) mediator case.

considered here, the dijet search is already limited by the systematic uncertainty on the background spectra. Thus, increasing the luminosity to 300 fb^{-1} or 3000 fb^{-1} does not allow to probe smaller couplings to quarks than those already excluded. For heavier mediators, increasing the luminosity does allow to probe sizeable portions of currently unconstrained parameter space.

Considering (axial-)vector mediators, cf. fig. 5, we find that at mediator masses of $m_{\text{med}} \sim 3.5 \text{ TeV}$ a signal could be discovered with a significance of at least 5σ if the coupling to quarks is larger than $g_q \sim 0.2$. Recall that the 36 fb^{-1} data excludes couplings larger than $g_q \sim 0.4$ for such mediator masses, while the 78 fb^{-1} data excludes couplings larger

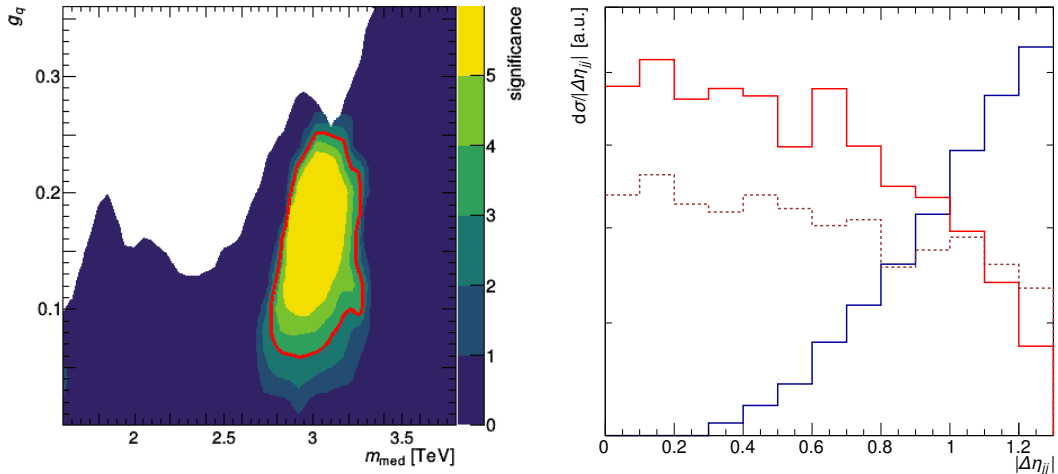


Figure 7: *Left:* Potential for parameter reconstruction if a signal from a vector mediator with a true mass of $m_{\text{med}} = 3.0$ TeV coupling to quarks only with $g_q = 0.2$ is observed at the HL-LHC. The color scale shows the expected significance Z with which the background only hypothesis can be rejected in favor of a hypothetical signal at a given point in parameter space based on data generated for the true signal and assuming a luminosity of 3000 fb^{-1} . The red line shows the 3σ error ellipse for parameter reconstruction. *Right:* Angular distribution $d\sigma/d|\Delta\eta_{jj}|$ of the dijet spectra for the SM background (solid blue), a scalar mediator (solid red), and a vector mediator (dashed burgundy). Note that the spectra are not shown to scale in order to emphasize the differences in shape. Both signal spectra are for $m_{\text{med}} = 2$ TeV and a decay width of $\Gamma_{\text{med}}/m_{\text{med}} = 0.05$. We consider only events near the resonance, $1.5 \text{ TeV} < m_{jj} < 2.5 \text{ TeV}$. Note that both background and signal events have been generated with our MadGraph instead of our default WHIZARD tool chain.

than $g_q \sim 0.25$. In the absence of a signal (and assuming that “discovery” and exclusion limits are comparable), 300 fb^{-1} (3000 fb^{-1}) of data would allow to exclude couplings larger than $g_q \sim 0.25$ ($g_q \sim 0.1$) at 95% C.L. for (axial-)vector mediators.⁴

For (pseudo)scalar mediators, cf. fig. 6, we find similar increases in sensitivity with respect to current limits. For mediators with mass $m_{\text{med}} \sim 3.5$ TeV the HL-LHC with 3000 fb^{-1} of data would allow for a detection with a significance of at least 5σ if the coupling to quarks is larger than $g_q \sim 0.3$. In the absence of a signal, the HL-LHC could exclude (pseudo)scalar mediators with masses of $m_{\text{med}} \sim 3.5$ TeV at 95% C.L. if the coupling to quarks is larger than $g_q \sim 0.2$ (again assuming that “discovery” and exclusion limits are comparable).

7 Parameter Reconstruction

In this section, we study how well the parameters of a simplified model could be reconstructed at the HL-LHC in case of a significant future discovery. Thus, we shift from projecting discovery/exclusion limits to parameter reconstruction. Confidence regions for parameter reconstruction are computed as in the case of sensitivity projections, cf. section 4, except that the profile likelihood ratio in eq. (4.4) is now calculated from the dataset $n_i = b_i(\boldsymbol{\theta}_{\text{bf}}) + \bar{s}_i$, where \bar{s}_i is the number of dijet events in the i -th mass bin for the true signal parameters m_{med} , g_q , and Γ_{med} .

As an illustrative example, in the left panel of fig. 7 we show the prospects for parameter reconstruction for the benchmark case of a vector mediator with a true mass of $m_{\text{med}} = 3.0$ TeV coupling only to quarks with strength $g_q = 0.20$ at the HL-LHC. These results indicate that for this parameter point, the mass could be reconstructed with a relative error of $\lesssim 10\%$ while the coupling strength could be reconstructed to $g_q \sim 0.18_{-0.10}^{+0.05}$. The best fit mass is $m_{\text{med}} = 3.05$ TeV. Not surprisingly, the relative error on the mediator mass, fixed by the location of the excess over the background in the m_{jj} direction, is smaller than the relative error on g_q which is determined by measuring the cross-section of the signal.

Differentiating different simplified models is difficult based on the differential dijet spectra with respect to the invariant mass $d\sigma/dm_{jj}$ discussed until here. This is because hadronization effects as well as the finite energy resolution of a real detector like CMS make it challenging to observe the minute differences in the spectra from different models. However, the dijet production cross sections have different dependence on the scattering angle for the different mediator cases considered here. Such dependence can be exploited by considering double differential dijet spectra $d^2\sigma/dm_{jj}d\Delta\eta_{jj}$, where $\Delta\eta_{jj}$ is the pseudorapidity difference between the two widejets. In the right panel of fig. 7 we show the $d\sigma/d|\Delta\eta_{jj}|$ distribution of the SM background and those for a scalar and vector mediator in comparison. The signal and background spectra shown in that panel are simulated with our `MadGraph` tool chain described in section 3 instead of our default `WHIZARD` tool chain. This figure shows that the angular distributions can in principle be used for distinguishing different simplified models. Further, considering the differences in the angular distributions between the signal and background spectra, the sensitivity of dijet searches may be further enhanced with respect to the results shown in section 5 and section 6 by using angular information.

Although seemingly promising, an analysis extending the sensitivity of dijet searches for simplified models with angular information is beyond the scope of this work. Note that both the ATLAS and the CMS collaboration have used angular information in dijet searches for BSM physics [36–39]. Regarding differentiating different simplified models in case of a discovery, calculations based on a naive profile likelihood indicate that the number of events in the region of parameter space not already excluded by current limits would not suffice to differentiate models. However, a more sophisticated analysis with optimized selection cuts may yield more promising results. We leave such investigations for future work.

⁴Recall that a 95% C.L. exclusion limit corresponds to a significance of $Z = 1.64$.

8 Conclusions

We presented a reanalysis of the latest results from CMS dijet searches for an integrated luminosity of 36 fb^{-1} together with preliminary results for 78 fb^{-1} in the framework of simplified models for (scalar, fermionic and vector) DM interacting with quarks through the exchange of a scalar, pseudoscalar, vector or pseudovector mediator particle [12, 30]. Within the same framework, we also projected the sensitivity of dijet searches in future LHC runs, assuming that the selection cuts will remain unchanged with respect to those employed in the current dijet analyses, and rescaling our background fit to the 36 fb^{-1} CMS dataset described in section 3.1 accordingly. Finally, we also studied how well the parameters of a simplified model could be reconstructed in case of a significant future discovery at the HL-LHC.

From our reanalysis of the latest results from CMS dijet searches, we obtained 95 % C.L. exclusion limits on the mediator coupling to quarks as a function of the mediator mass for spin 0 and spin 1 mediators. Exclusion limits for scalar and pseudoscalar mediators were derived here for the first time. In this study, we considered two cases separately: 1) The mediator couples to quarks only, and thus its width, Γ_{med} , is determined by m_{med} and g_q . 2) Γ_{med} is a free parameter to account for additional decay channels of the mediator, e.g. into pairs of DM particles. For both the 36 fb^{-1} and the 78 fb^{-1} data, the limits that we obtained are within 1σ of the respective expected limits, indicating that both CMS datasets show no evidence for a dijet signal in the simplified model framework. Comparing the results from the 36 fb^{-1} data to those from the 78 fb^{-1} data, we found that the larger luminosity allows for more stringent exclusion limits, but only for large mediator masses where exclusion limits are limited by statistical rather than systematic errors.

When projecting the sensitivity of dijet searches in future LHC runs, we focused on two benchmark cases: 1) An integrated luminosity of 300 fb^{-1} as expected to be collected at the end of Run 3 of the LHC in 2023. 2) An integrated luminosity of 3000 fb^{-1} as expected to be collected by ~ 2037 after the high luminosity upgrade of the LHC. We obtained sensitivity projections under the assumption that the mediator couples to quarks only, and thus its width is determined by m_{med} and g_q only. The improvements found with respect to the currently excluded regions in the parameter space of simplified models is rather small for mediator masses $m_{\text{med}} \sim 1.6 \text{ TeV}$ – where the dijet searches are already limited by the systematic uncertainty on the background spectra – but they become significant for heavier mediators, where dijet searches are limited by statistics. We found that in this latter case sizable portions of currently unconstrained parameter space will be within reach at the HL-LHC.

Assessing how well the parameters of a given simplified model can be reconstructed in case of a significant future discovery at the HL-LHC, we focused on a single benchmark case where a vector mediator with a true mass of $m_{\text{med}} = 3.0 \text{ TeV}$ couples only to quarks with strength $g_q = 0.20$. In this specific case, we found that the mediator mass could be reconstructed with a relative error of $\lesssim 10\%$, while the reconstructed coupling strength was $g_q \sim 0.2_{-0.10}^{+0.05}$.

Finally, we also explored the possibility of discriminating different mediator scenarios by extending the sensitivity of dijet searches for simplified models through the use of angular information. The feasibility of this approach relies on the fact that dijet production cross sections at the LHC have a different dependence on the scattering angle for the different mediator cases considered here. Although seemingly promising, we left such investigation for future work.

Acknowledgments

We thank Jan Conrad and Katherine Freese for their contribution to the early stages of this project. We are grateful to Caterina Doglioni and Felix Kahlhoefer for useful insights into how to model dijet signal and background events at the LHC. Finally, it is a pleasure to thank Kåre Fridell and Vanessa Zema for helpful discussions on non-relativistic effective theories and simplified models for dark matter. This work is performed within the Swedish Consortium for Dark Matter Direct Detection (SweDCube), and was supported by the Knut and Alice Wallenberg Foundation (PI, Jan Conrad), by the Vetenskapsrådet (Swedish Research Council) through contract No. 638-2013-8993, and the Oskar Klein Centre for Cosmoparticle Physics.

A Signal fit and spectra

In this appendix we list the fit parameters corresponding to eq. (3.3) for selected parameter points for a vector, axial-vector, scalar and pseudoscalar mediator in tab. 1-4, which can be used for further analysis without the need to simulate the signal processes again. We assume universal couplings to the quarks and no additional decay channels for the mediator. In fig. 8 we show signal spectra and the corresponding fits assuming a vector mediator for illustration for a subset of parameter points.

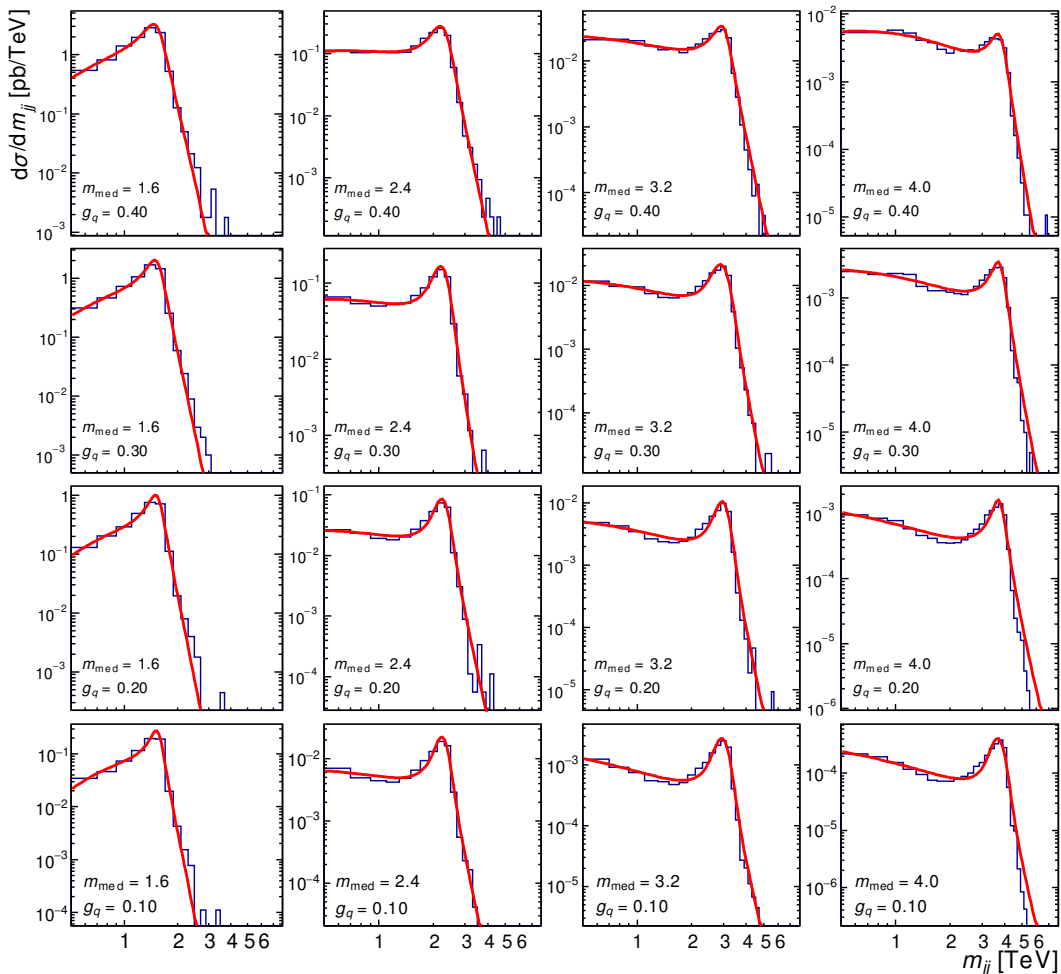


Figure 8: Simulated signal spectra (blue histogram) and corresponding fit (eq. (3.3), red line) for several parameter points in the vector mediator case assuming that the mediator couples to quarks only. The mediator mass m_{med} in TeV and the coupling to quarks g_q are listed in the respective panels. Note that the scale of the y -axis differs between the respective panels. Panels in the same column share the value for the mediator mass, while panels in the same row share the value for the coupling of the mediator to quarks. The signal spectra for the scalar, pseudoscalar, and axial-vector case are similar to the vector mediator case shown here.

$\frac{m_{\text{med}}}{\text{GeV}}$	g_q	$\frac{p_0}{\text{fb/GeV}}$	$\frac{p_1}{\text{GeV}}$	$\frac{p_2}{\text{GeV}}$	$\frac{p_3}{\text{GeV}}$	p_4	p_5
1600	0.05	5.43357×10^5	282.612	1546.450	6.05008×10^{-1}	-9.86023	4.53496
1600	0.10	3.68206×10^6	270.945	1551.107	4.54318	-10.41522	4.79370
1600	0.15	5.97351×10^5	301.361	1532.236	2.73148×10^{-1}	-7.71246	3.22862
1600	0.20	3.12253×10^6	318.096	1542.951	5.62014×10^{-1}	-8.79416	3.96967
1600	0.25	2.80549×10^6	334.138	1538.902	1.51016	-8.24228	3.62487
1600	0.30	2.72932×10^6	363.043	1535.325	4.41062×10^{-1}	-7.83232	3.45908
1600	0.35	7.31285×10^6	383.076	1541.762	1.57555×10^{-1}	-8.53564	3.94213
1600	0.40	2.15259×10^6	429.462	1523.177	6.49771×10^{-1}	-6.95947	3.16951
1600	0.45	1.60324×10^6	466.606	1516.691	6.91752×10^{-1}	-6.44059	2.90848
2000	0.05	3.93500×10^3	296.440	1914.366	6.69305×10^1	-6.05549	1.28131
2000	0.10	1.29671×10^4	325.795	1914.354	5.45899	-5.87183	1.16092
2000	0.15	4.22177×10^4	330.627	1913.267	9.58694×10^{-1}	-6.23354	1.44063
2000	0.20	4.42496×10^4	285.340	1916.568	8.51642×10^1	-5.71231	0.92549
2000	0.25	1.52420×10^5	354.664	1920.033	1.30534×10^{-1}	-6.53100	1.60575
2000	0.30	2.33439×10^5	396.727	1928.272	5.59112×10^{-1}	-6.56657	1.75425
2000	0.35	1.41725×10^5	389.932	1899.717	7.21201×10^1	-5.73011	1.31740
2000	0.40	1.15572×10^5	464.323	1899.313	7.60358×10^1	-5.22676	1.17490
2000	0.45	3.06705×10^5	483.640	1913.765	9.87537×10^1	-6.00754	1.63213
2400	0.05	5.59414×10^2	346.703	2286.943	5.36397×10^{-1}	-5.13274	0.45203
2400	0.10	2.65611×10^3	303.767	2293.762	9.87371×10^1	-5.32930	0.44016
2400	0.15	1.05415×10^5	346.163	2305.575	2.75506×10^{-1}	-8.24659	2.31603
2400	0.20	1.26468×10^4	317.490	2297.326	1.03349×10^2	-5.51095	0.54670
2400	0.25	1.48876×10^4	331.346	2287.527	1.16979×10^2	-5.22197	0.38458
2400	0.30	3.39259×10^4	370.681	2293.786	1.16980×10^2	-5.71855	0.70399
2400	0.35	2.84299×10^4	470.683	2287.043	8.57590×10^1	-5.17932	0.62286
2400	0.40	5.18226×10^4	465.051	2292.506	1.13611×10^2	-5.49941	0.78452
2400	0.45	9.09806×10^4	540.594	2278.128	6.61869×10^1	-5.82709	1.13088
2800	0.05	9.68462×10^1	403.791	2661.798	3.55910×10^{-1}	-4.30635	-0.10629
2800	0.10	3.52737×10^1	441.458	2632.252	1.80878×10^{-2}	-1.84460	-1.43052
2800	0.15	2.13433×10^3	325.072	2667.846	1.34877×10^2	-5.27060	0.20649
2800	0.20	3.08903×10^3	353.656	2662.574	1.41426×10^2	-5.06439	0.12572
2800	0.25	2.94567×10^3	493.844	2649.974	3.02310×10^1	-4.50275	0.07269
2800	0.30	8.64732×10^3	422.868	2663.485	1.40325×10^2	-5.25596	0.33216
2800	0.35	1.22637×10^4	463.833	2655.475	1.45209×10^2	-5.26814	0.43607
2800	0.40	3.60051×10^4	460.848	2671.361	1.64151×10^2	-6.15834	0.80327
2800	0.45	3.57938×10^4	539.634	2657.619	1.58678×10^2	-5.85375	0.82222
3200	0.05	5.39058×10^1	327.513	3036.885	1.61773×10^2	-4.70282	-0.27394
3200	0.10	1.88780×10^2	338.731	3027.014	1.71367×10^2	-4.52350	-0.28728
3200	0.15	4.49073×10^2	347.328	3026.539	1.57853×10^2	-4.58585	-0.29001
3200	0.20	1.74776×10^3	374.101	3039.745	1.48830×10^2	-5.40473	0.16547
3200	0.25	1.51618×10^3	541.023	3038.987	1.14012×10^1	-4.74749	0.12095
3200	0.30	4.56523×10^3	427.180	3025.041	1.88443×10^2	-5.53016	0.29508
3200	0.35	1.33440×10^4	449.081	3061.446	1.97443×10^2	-6.35182	0.64895
3200	0.40	1.38316×10^3	731.751	2980.596	2.82204×10^{-1}	-3.64044	-0.37884
3200	0.45	2.75520×10^4	549.746	3076.220	1.85274×10^2	-6.56618	0.82067
3600	0.05	2.34396×10^1	314.122	3394.798	2.22928×10^2	-4.71483	-0.33471
3600	0.10	5.34590×10^1	502.538	3411.750	1.13208×10^1	-4.09866	-0.33191
3600	0.15	2.32948×10^2	398.755	3400.779	1.86235×10^2	-4.83444	-0.20208
3600	0.20	3.29207×10^2	559.950	3413.971	1.12794×10^1	-4.57082	-0.15471
3600	0.25	1.90275×10^3	410.062	3408.040	2.13609×10^2	-5.94925	0.27389
3600	0.30	2.72615×10^3	525.893	3414.426	1.67678×10^2	-5.88904	0.42731
3600	0.35	3.57320×10^3	544.856	3403.284	1.84992×10^2	-5.86356	0.34646
3600	0.40	7.04552×10^3	709.095	3421.111	2.01746	-6.25530	0.67730
3600	0.45	7.93546×10^3	751.939	3408.811	1.95324	-6.14830	0.56989
4000	0.05	9.44562	345.979	3773.699	2.37458×10^2	-4.67954	-0.41206
4000	0.10	2.41455×10^1	545.594	3775.325	1.12972×10^1	-4.17045	-0.37513
4000	0.15	6.16856×10^1	615.578	3767.127	1.51870×10^1	-4.31146	-0.27883
4000	0.20	3.60401×10^2	392.794	3771.092	2.45381×10^2	-5.55022	-0.01319
4000	0.25	4.91869×10^2	623.840	3790.407	1.06424×10^1	-5.39636	0.12325
4000	0.30	3.49562×10^3	425.593	3800.649	2.52977×10^2	-7.06489	0.61386
4000	0.35	4.87073×10^3	561.559	3803.419	2.05524×10^2	-7.06022	0.74989
4000	0.40	2.13261×10^4	493.077	3843.718	2.66624×10^2	-8.42267	1.11784
4000	0.45	2.21280×10^1	366.246	3812.175	1.01225×10^3	-0.81612	-2.05223

Table 1: Fit values for the signal for a vector mediator.

$\frac{m_{\text{med}}}{\text{GeV}}$	g_q	$\frac{p_0}{\text{fb/GeV}}$	$\frac{p_1}{\text{GeV}}$	$\frac{p_2}{\text{GeV}}$	$\frac{p_3}{\text{GeV}}$	p_4	p_5
1600	0.05	7.22471×10^5	261.524	1548.861	1.74381×10^{-1}	-10.16781	4.67876
1600	0.10	2.07119×10^6	268.846	1546.786	3.15229×10^1	-9.83374	4.40196
1600	0.15	2.11243×10^6	291.078	1540.869	7.29639×10^{-2}	-9.00341	3.99077
1600	0.20	8.60864×10^4	320.473	1518.118	3.48798×10^{-2}	-5.16218	1.55340
1600	0.25	4.40812×10^6	329.067	1543.481	1.04830×10^{-1}	-8.72852	3.93547
1600	0.30	4.12705×10^5	355.997	1527.036	3.22511×10^{-1}	-5.93029	2.10857
1600	0.35	1.72044×10^6	384.237	1524.828	6.08628	-7.02556	3.10563
1600	0.40	3.70595×10^6	405.785	1528.178	5.11102×10^{-2}	-7.55400	3.47877
1600	0.45	4.99712×10^6	443.776	1520.235	4.32108×10^1	-7.56885	3.71086
2000	0.05	4.35505×10^3	277.945	1919.574	7.47707×10^1	-6.20024	1.21594
2000	0.10	1.09272×10^4	273.862	1913.306	7.75026×10^1	-5.70715	0.93570
2000	0.15	3.98160×10^4	319.899	1915.552	4.38707×10^{-2}	-6.20363	1.30892
2000	0.20	3.26680×10^4	318.109	1908.711	6.48833×10^1	-5.38423	0.87602
2000	0.25	7.34075×10^4	345.473	1906.653	7.02021×10^1	-5.75907	1.18835
2000	0.30	1.01296×10^5	344.519	1906.232	8.46143×10^1	-5.71224	1.20405
2000	0.35	1.08614×10^5	381.387	1898.578	7.89286×10^1	-5.47725	1.11100
2000	0.40	1.43755×10^5	463.510	1899.285	5.29813	-5.45658	1.31249
2000	0.45	3.63814×10^5	515.704	1917.195	5.90913	-6.14050	1.82965
2400	0.05	7.98471×10^2	311.333	2299.673	7.74125×10^1	-5.49934	0.58689
2400	0.10	2.71015×10^3	268.995	2284.975	1.15770×10^2	-5.32861	0.39071
2400	0.15	7.57449×10^3	309.078	2296.197	9.52726×10^1	-5.57612	0.54633
2400	0.20	8.26778×10^3	294.482	2285.577	1.37785×10^2	-5.08423	0.23697
2400	0.25	1.18606×10^4	361.258	2280.840	1.03076×10^2	-4.99099	0.34222
2400	0.30	1.21103×10^4	406.246	2280.300	1.00911×10^2	-4.61060	0.21267
2400	0.35	4.03849×10^4	414.390	2286.582	1.15030×10^2	-5.54181	0.77573
2400	0.40	2.62471×10^4	478.025	2272.751	1.06082×10^2	-4.81027	0.40772
2400	0.45	4.54467×10^4	534.710	2264.979	8.72913×10^1	-5.11589	0.70109
2800	0.05	7.99366×10^1	414.681	2659.754	6.63948	-4.09824	-0.16491
2800	0.10	6.89306×10^2	329.295	2660.279	1.25516×10^2	-4.92936	0.03736
2800	0.15	1.44819×10^3	334.034	2655.127	1.35885×10^2	-4.84239	0.00717
2800	0.20	3.05854×10^3	330.974	2669.421	1.61384×10^2	-5.02812	0.07033
2800	0.25	3.06514×10^3	458.479	2656.949	3.60328×10^1	-4.55270	0.04771
2800	0.30	1.25037×10^4	404.238	2665.745	1.56778×10^2	-5.64260	0.52216
2800	0.35	1.43054×10^4	418.868	2659.954	1.71818×10^2	-5.48547	0.40376
2800	0.40	2.09166×10^4	460.904	2665.642	1.62621×10^2	-5.61546	0.48066
2800	0.45	4.56375×10^4	524.035	2676.133	1.62444×10^2	-6.16940	0.86434
3200	0.05	5.19532×10^1	327.093	3032.071	1.62118×10^2	-4.64117	-0.25025
3200	0.10	1.65045×10^2	372.236	3029.917	1.33993×10^2	-4.36593	-0.28234
3200	0.15	7.38357×10^2	319.697	3039.065	1.90814×10^2	-5.12650	-0.08700
3200	0.20	1.41773×10^3	348.891	3028.817	1.94602×10^2	-5.19704	-0.00471
3200	0.25	2.00614×10^3	459.088	3041.581	1.30894×10^2	-5.04587	0.15280
3200	0.30	2.87860×10^3	460.310	3028.983	1.74669×10^2	-5.04724	0.05934
3200	0.35	1.17676×10^4	472.940	3055.053	1.61058×10^2	-6.24580	0.59337
3200	0.40	1.33870×10^4	451.069	3041.077	2.36791×10^2	-6.07216	0.48080
3200	0.45	4.25546×10^4	528.994	3072.086	2.06203×10^2	-7.06165	1.04056
3600	0.05	9.58131	514.402	3403.385	1.50979×10^1	-3.74820	-0.48711
3600	0.10	1.09692×10^2	381.489	3413.096	1.77672×10^2	-4.88150	-0.14278
3600	0.15	2.79017×10^2	373.126	3421.325	1.99754×10^2	-4.99646	-0.13504
3600	0.20	7.45370×10^2	438.439	3403.592	1.75254×10^2	-5.41304	0.15901
3600	0.25	7.33213×10^2	589.579	3402.359	1.43299×10^1	-4.89556	0.04284
3600	0.30	3.71762×10^3	495.444	3413.360	1.68682×10^2	-6.23221	0.53117
3600	0.35	4.17688×10^3	561.193	3406.906	1.58027×10^2	-5.98192	0.45757
3600	0.40	1.54159×10^4	689.369	3426.519	1.09322×10^1	-7.08610	1.07841
3600	0.45	3.87852×10^4	519.889	3458.267	2.51578×10^2	-7.92126	1.13583
4000	0.05	8.64212	362.063	3779.525	2.29793×10^2	-4.60167	-0.43791
4000	0.10	2.04269×10^1	552.916	3781.710	1.12972×10^1	-3.99881	-0.45205
4000	0.15	1.09514×10^2	426.865	3789.181	2.12923×10^2	-4.92267	-0.21230
4000	0.20	1.63621×10^2	618.757	3787.468	1.11946×10^1	-4.70702	-0.11656
4000	0.25	1.23778×10^3	442.761	3799.985	2.30898×10^2	-6.38462	0.36140
4000	0.30	4.78918×10^3	423.961	3822.639	2.53584×10^2	-7.43131	0.74585
4000	0.35	2.22022×10^3	708.023	3793.527	1.68849×10^1	-6.23818	0.47919
4000	0.40	1.21003×10^4	562.075	3832.288	2.70009×10^2	-7.80832	0.95964
4000	0.45	4.12952×10^4	481.870	3843.512	3.24035×10^2	-8.87296	1.28449

Table 2: Fit values for the signal for an axial-vector mediator.

$\frac{m_{\text{med}}}{\text{GeV}}$	g_q	$\frac{p_0}{\text{fb/GeV}}$	$\frac{p_1}{\text{GeV}}$	$\frac{p_2}{\text{GeV}}$	$\frac{p_3}{\text{GeV}}$	p_4	p_5
1600	0.05	3.38630×10^5	273.491	1549.757	1.09411×10^{-2}	-9.95714	4.41330
1600	0.10	1.12530×10^6	284.372	1547.002	1.73230×10^{-1}	-9.73847	4.45723
1600	0.15	2.98621×10^6	297.111	1546.167	2.60991	-9.90257	4.57945
1600	0.20	2.32618×10^6	311.388	1543.277	6.38288×10^{-1}	-9.05902	4.07785
1600	0.25	5.28996×10^5	356.664	1529.356	9.28856×10^{-1}	-7.09259	2.91046
1600	0.30	2.02690×10^6	414.445	1532.818	1.01555	-8.03318	3.83000
1600	0.35	8.63365×10^5	439.023	1518.524	1.52358	-6.83339	3.21348
1600	0.40	1.55652×10^6	507.714	1519.528	4.36909×10^{-1}	-7.13384	3.54007
1600	0.45	1.78774×10^6	558.898	1507.142	3.07215×10^{-1}	-7.03292	3.59298
2000	0.05	2.21953×10^3	283.601	1918.759	5.51110×10^1	-6.03719	1.11727
2000	0.10	1.35137×10^4	273.508	1919.628	7.47989×10^1	-6.49663	1.35314
2000	0.15	2.06325×10^4	336.546	1920.426	4.69462	-6.07970	1.29375
2000	0.20	1.49975×10^4	298.465	1902.048	1.03528×10^2	-5.15059	0.70149
2000	0.25	3.59638×10^4	325.094	1912.701	1.06304×10^2	-5.60558	1.03251
2000	0.30	6.97361×10^4	408.102	1916.164	4.34773	-5.89053	1.33345
2000	0.35	8.12983×10^4	466.877	1900.340	1.15069×10^1	-5.70185	1.38174
2000	0.40	9.72522×10^4	573.844	1892.438	1.57794	-5.56130	1.57844
2000	0.45	2.59981×10^5	574.148	1928.985	6.70369×10^1	-6.38070	1.91570
2400	0.05	2.76182×10^1	372.769	2268.313	7.73057×10^{-2}	-2.57987	-0.91755
2400	0.10	6.84684×10^2	338.406	2280.030	6.00796×10^1	-4.42790	0.02632
2400	0.15	3.38227×10^3	297.440	2295.105	1.05922×10^2	-5.30579	0.32251
2400	0.20	6.48120×10^3	355.433	2295.967	9.69624×10^1	-5.37400	0.55380
2400	0.25	2.02793×10^4	380.192	2306.561	9.34515×10^1	-6.08384	0.98010
2400	0.30	2.29152×10^4	401.847	2291.080	1.29997×10^2	-5.84090	0.86003
2400	0.35	1.71312×10^4	557.853	2282.679	5.49647	-5.16012	0.76220
2400	0.40	4.25894×10^4	538.422	2293.188	1.08403×10^2	-5.86726	1.04146
2400	0.45	6.97560×10^4	665.235	2290.991	2.05692	-6.09851	1.37050
2800	0.05	6.59744×10^1	297.030	2658.200	1.39159×10^2	-4.49309	-0.31930
2800	0.10	4.02940×10^2	417.669	2670.717	5.17397	-4.88655	0.23576
2800	0.15	5.56311×10^2	444.785	2653.833	5.64693	-4.38572	-0.00415
2800	0.20	2.43438×10^3	329.094	2665.414	1.60913×10^2	-5.37478	0.22541
2800	0.25	5.38415×10^3	369.633	2665.801	1.71251×10^2	-5.73452	0.46508
2800	0.30	1.79229×10^2	659.302	2556.159	3.73320×10^{-1}	-1.71914	-1.23592
2800	0.35	1.05995×10^4	524.597	2667.605	1.57665×10^2	-5.66616	0.68458
2800	0.40	6.34529×10^2	809.514	2553.878	5.92711×10^{-2}	-2.37558	-0.75458
2800	0.45	5.85787×10^4	548.858	2709.360	2.27062×10^2	-7.03406	1.24782
3200	0.05	1.93562×10^1	453.534	3034.438	2.20013	-4.13108	-0.24153
3200	0.10	1.65120×10^2	348.334	3035.386	1.68005×10^2	-4.96464	-0.09652
3200	0.15	2.46862×10^2	496.400	3038.515	2.19229	-4.48388	-0.06645
3200	0.20	1.08979×10^3	401.542	3035.259	1.62011×10^2	-5.45358	0.21655
3200	0.25	5.76739×10^2	595.962	3014.854	1.00286×10^1	-4.29130	-0.14619
3200	0.30	7.00933×10^1	778.269	2950.095	4.70260×10^{-1}	-1.73439	-1.27694
3200	0.35	4.12125×10^3	702.643	3023.723	5.02951	-5.63244	0.56299
3200	0.40	9.92050×10^3	636.208	3049.896	2.19994×10^2	-6.31735	0.76767
3200	0.45	1.84701×10^4	799.165	3044.615	1.42380×10^2	-6.69027	1.08946
3600	0.05	1.50667×10^1	367.089	3411.342	1.78689×10^2	-4.80561	-0.19737
3600	0.10	4.23942×10^1	474.500	3409.443	7.85452×10^1	-4.44915	-0.21250
3600	0.15	5.60645×10^1	572.187	3390.615	4.92089	-3.87421	-0.48165
3600	0.20	5.15207×10^2	406.564	3413.827	2.29368×10^2	-5.59177	0.12257
3600	0.25	8.70832×10^2	645.798	3419.739	9.93860	-5.64058	0.39936
3600	0.30	1.77505×10^3	699.554	3423.577	2.89978	-5.99481	0.57158
3600	0.35	3.30752×10^3	738.341	3404.719	9.98038	-6.31467	0.69214
3600	0.40	9.61949×10^3	793.028	3442.838	1.31419	-7.15104	1.04170
3600	0.45	1.31058×10^4	894.687	3437.337	1.00726×10^2	-7.23459	1.12404
4000	0.05	5.17696	382.467	3782.988	2.19348×10^2	-4.58906	-0.38007
4000	0.10	1.70025×10^1	562.946	3794.446	1.28497×10^{-1}	-4.37029	-0.29736
4000	0.15	3.39362×10^1	628.036	3766.378	5.12344	-4.20579	-0.30615
4000	0.20	1.41861×10^1	788.761	3750.000	2.04301×10^{-1}	-2.73831	-1.02880
4000	0.25	3.47830×10^2	702.052	3771.040	1.00286×10^1	-5.54813	0.21768
4000	0.30	9.62600×10^2	787.579	3784.294	1.67365	-6.21644	0.54180
4000	0.35	2.70986×10^3	802.826	3802.423	4.43008	-6.96405	0.81097
4000	0.40	6.01189×10^3	896.294	3806.740	1.30173	-7.56984	1.03734
4000	0.45	7.01371×10^3	1086.105	3823.621	1.07115×10^1	-7.50088	1.01614

Table 3: Fit values for the signal for a scalar mediator.

m_{med} GeV	g_q	$\frac{p_0}{\text{fb/GeV}}$	$\frac{p_1}{\text{GeV}}$	$\frac{p_2}{\text{GeV}}$	$\frac{p_3}{\text{GeV}}$	p_4	p_5
1600	0.05	1.71887×10^5	266.804	1552.146	3.80328×10^{-1}	-9.26805	3.87058
1600	0.10	5.19261×10^4	283.560	1532.086	9.83644×10^{-3}	-6.59533	2.38065
1600	0.15	1.02629×10^6	296.175	1549.389	2.43648×10^{-3}	-8.81629	3.82032
1600	0.20	2.29493×10^5	326.132	1525.132	3.82526×10^{-1}	-6.70108	2.54281
1600	0.25	1.19460×10^6	346.035	1529.321	3.15404×10^1	-7.91232	3.45775
1600	0.30	3.60679×10^5	396.829	1517.493	2.04181	-6.29540	2.63030
1600	0.35	1.95418×10^6	449.179	1533.890	1.47218×10^{-2}	-7.70149	3.63592
1600	0.40	1.37037×10^6	532.747	1513.991	4.03759	-6.98750	3.51866
1600	0.45	2.26351×10^6	541.513	1513.512	4.86235×10^{-1}	-7.25564	3.72507
2000	0.05	1.27719×10^3	276.536	1913.254	7.82957×10^1	-5.46148	0.82683
2000	0.10	6.77471×10^1	362.581	1868.981	4.62106×10^{-2}	-1.06832	-1.62934
2000	0.15	1.38323×10^4	336.663	1906.353	1.39983×10^1	-5.63581	1.08759
2000	0.20	3.48834×10^4	365.236	1910.752	5.10019	-5.98936	1.39631
2000	0.25	5.72775×10^4	339.600	1911.992	8.27745×10^1	-6.09012	1.29559
2000	0.30	7.44500×10^4	393.038	1912.306	7.31368×10^1	-5.96101	1.39842
2000	0.35	5.84644×10^4	487.655	1898.756	2.85123×10^1	-5.34587	1.20385
2000	0.40	1.90144×10^5	569.310	1913.505	8.83831×10^{-1}	-6.27267	1.92906
2000	0.45	5.43384×10^4	645.666	1890.961	8.38206×10^{-1}	-4.71444	1.16712
2400	0.05	5.37168×10^2	280.088	2294.186	1.02472×10^2	-5.66324	0.56621
2400	0.10	1.88890×10^3	292.382	2292.577	1.05147×10^2	-5.51003	0.53767
2400	0.15	1.86916×10^3	392.341	2279.426	5.49679	-4.65407	0.28131
2400	0.20	3.93111×10^3	335.391	2275.744	1.18549×10^2	-4.85866	0.18788
2400	0.25	1.21202×10^4	371.786	2290.595	1.24540×10^2	-5.55269	0.64554
2400	0.30	1.23655×10^4	428.401	2289.473	1.15821×10^2	-5.18564	0.54813
2400	0.35	2.49388×10^4	518.589	2281.783	8.60692×10^1	-5.56302	0.96164
2400	0.40	5.36880×10^4	594.434	2303.149	1.81313	-6.09594	1.23979
2400	0.45	6.26662×10^4	690.873	2294.062	9.41360×10^1	-5.97086	1.37238
2800	0.05	5.78706×10^1	408.856	2661.673	1.62277	-4.32451	-0.09269
2800	0.10	1.80086×10^2	418.365	2646.004	7.47397	-4.05888	-0.22052
2800	0.15	8.96101×10^2	434.295	2669.675	9.07279	-4.89253	0.20762
2800	0.20	1.46927×10^3	472.731	2660.955	5.94141	-4.78727	0.19150
2800	0.25	2.64937×10^3	510.572	2654.867	5.13110	-4.91616	0.35001
2800	0.30	6.32701×10^3	441.146	2670.388	1.69019×10^2	-5.51656	0.39329
2800	0.35	9.54524×10^3	616.327	2649.467	7.16162×10^{-2}	-5.54899	0.71668
2800	0.40	1.42616×10^4	643.059	2662.391	1.36427×10^2	-5.69222	0.79505
2800	0.45	3.12298×10^4	779.067	2700.072	1.68051	-6.28460	1.11991
3200	0.05	2.02864×10^1	465.864	3030.027	1.83473×10^{-1}	-4.16929	-0.18236
3200	0.10	9.82148×10^1	396.659	3029.968	1.23992×10^2	-4.38838	-0.24654
3200	0.15	2.02446×10^2	509.818	3032.444	1.00399×10^1	-4.27369	-0.13497
3200	0.20	4.04878×10^2	535.512	3027.933	7.18709	-4.39688	-0.10830
3200	0.25	2.78279×10^3	463.030	3048.710	1.50522×10^2	-5.99517	0.49177
3200	0.30	3.08515×10^3	638.072	3033.206	1.12689×10^1	-5.63909	0.59223
3200	0.35	4.16549×10^3	725.028	3032.567	1.02021×10^{-2}	-5.62205	0.60431
3200	0.40	2.68592×10^4	554.152	3082.207	2.15230×10^2	-7.41210	1.15787
3200	0.45	1.02845×10^5	460.577	3129.373	2.98148×10^2	-8.67939	1.52798
3600	0.05	7.70261	519.734	3411.109	5.24471	-4.08693	-0.31523
3600	0.10	7.94554×10^1	341.434	3405.078	2.10733×10^2	-5.09566	-0.13925
3600	0.15	1.89137×10^2	389.034	3402.391	2.20977×10^2	-5.17022	-0.08975
3600	0.20	2.24845×10^2	605.387	3398.702	1.17278	-4.67205	-0.03972
3600	0.25	8.73285×10^2	514.405	3413.723	1.80299×10^2	-5.66116	0.24032
3600	0.30	5.33930×10^3	486.467	3439.010	2.47584×10^2	-7.22246	0.87564
3600	0.35	1.16349×10^4	493.622	3440.181	2.40164×10^2	-7.70719	1.04787
3600	0.40	5.75392×10^3	850.145	3427.450	1.10229×10^1	-6.62114	0.81555
3600	0.45	1.65576×10^4	783.363	3461.780	2.02893×10^2	-7.55571	1.10540
4000	0.05	9.13344	381.622	3789.547	2.00416×10^2	-5.17271	-0.07829
4000	0.10	1.64155×10^1	568.700	3791.270	9.68369×10^{-1}	-4.31143	-0.29259
4000	0.15	7.92659×10^1	431.948	3778.164	2.25907×10^2	-5.14046	-0.16394
4000	0.20	3.06745×10^2	480.655	3781.655	2.04211×10^2	-5.90642	0.25400
4000	0.25	3.80032×10^2	720.398	3771.032	1.00768×10^1	-5.62714	0.30185
4000	0.30	4.46817×10^3	491.297	3823.530	2.43861×10^2	-7.90173	0.98986
4000	0.35	4.17238×10^3	716.423	3834.021	1.44441×10^2	-7.48900	0.91814
4000	0.40	6.60943×10^3	886.825	3811.766	8.52635×10^1	-7.69392	1.07113
4000	0.45	1.40095×10^4	901.722	3802.722	8.10194×10^{-2}	-8.24594	1.25383

Table 4: Fit values for the signal for a pseudo-scalar mediator.

References

- [1] ATLAS collaboration, M. Aaboud et al., *Search for new phenomena in dijet events using 37 fb⁻¹ of pp collision data collected at $\sqrt{s} = 13$ TeV with the ATLAS detector*, *Phys. Rev.* **D96** (2017) 052004, [[1703.09127](#)].
- [2] CMS collaboration, *Searches for dijet resonances in pp collisions at $\sqrt{s} = 13$ TeV using data collected in 2016*, [CMS-PAS-EXO-16-056](#).
- [3] CMS collaboration, A. M. Sirunyan et al., *Search for narrow and broad dijet resonances in proton-proton collisions at $\sqrt{s} = 13$ TeV and constraints on dark matter mediators and other new particles*, *JHEP* **08** (2018) 130, [[1806.00843](#)].
- [4] CMS collaboration, *Searches for dijet resonances in pp collisions at $\sqrt{s} = 13$ TeV using the 2016 and 2017 datasets*, [CMS-PAS-EXO-17-026](#).
- [5] ATLAS collaboration, M. Aaboud et al., *Search for low-mass dijet resonances using trigger-level jets with the ATLAS detector in pp collisions at $\sqrt{s} = 13$ TeV*, *Phys. Rev. Lett.* **121** (2018) 081801, [[1804.03496](#)].
- [6] CMS collaboration, A. M. Sirunyan et al., *Search for narrow resonances in the b-tagged dijet mass spectrum in proton-proton collisions at $\sqrt{s} = 8$ TeV*, *Phys. Rev. Lett.* **120** (2018) 201801, [[1802.06149](#)].
- [7] ATLAS collaboration, *Search for dijet resonances in events with an isolated lepton using $\sqrt{s} = 13$ TeV proton-proton collision data collected by the ATLAS detector*, Tech. Rep. ATLAS-CONF-2018-015, CERN, Geneva, Jun, 2018.
- [8] ATLAS collaboration, M. Aaboud et al., *Search for light resonances decaying to boosted quark pairs and produced in association with a photon or a jet in proton-proton collisions at $\sqrt{s} = 13$ TeV with the ATLAS detector*, [1801.08769](#).
- [9] S. Baum, R. Catena and M. B. Krauss, *Impact of a XENONnT signal on LHC dijet searches*, to appear.
- [10] J. Abdallah et al., *Simplified Models for Dark Matter and Missing Energy Searches at the LHC*, [1409.2893](#).
- [11] O. Buchmueller, M. J. Dolan and C. McCabe, *Beyond Effective Field Theory for Dark Matter Searches at the LHC*, *JHEP* **01** (2014) 025, [[1308.6799](#)].
- [12] J. B. Dent, L. M. Krauss, J. L. Newstead and S. Sabharwal, *General analysis of direct dark matter detection: From microphysics to observational signatures*, *Phys. Rev.* **D92** (2015) 063515, [[1505.03117](#)].
- [13] M. T. Frandsen, F. Kahlhoefer, A. Preston, S. Sarkar and K. Schmidt-Hoberg, *LHC and Tevatron Bounds on the Dark Matter Direct Detection Cross-Section for Vector Mediators*, *JHEP* **07** (2012) 123, [[1204.3839](#)].
- [14] H. An, X. Ji and L.-T. Wang, *Light Dark Matter and Z' Dark Force at Colliders*, *JHEP* **07** (2012) 182, [[1202.2894](#)].
- [15] H. An, R. Huo and L.-T. Wang, *Searching for Low Mass Dark Portal at the LHC*, *Phys. Dark Univ.* **2** (2013) 50–57, [[1212.2221](#)].
- [16] B. A. Dobrescu and F. Yu, *Coupling-mass mapping of dijet peak searches*, *Phys. Rev.* **D88** (2013) 035021, [[1306.2629](#)], [Erratum: *Phys. Rev.* **D90**,no.7,079901(2014)].

- [17] A. Alves, S. Profumo and F. S. Queiroz, *The dark Z' portal: direct, indirect and collider searches*, *JHEP* **04** (2014) 063, [[1312.5281](#)].
- [18] G. Arcadi, Y. Mambrini, M. H. G. Tytgat and B. Zaldivar, *Invisible Z' and dark matter: LHC vs LUX constraints*, *JHEP* **03** (2014) 134, [[1401.0221](#)].
- [19] M. Chala, F. Kahlhoefer, M. McCullough, G. Nardini and K. Schmidt-Hoberg, *Constraining Dark Sectors with Monojets and Dijets*, *JHEP* **07** (2015) 089, [[1503.05916](#)].
- [20] M. Fairbairn, J. Heal, F. Kahlhoefer and P. Tunney, *Constraints on Z' models from LHC dijet searches and implications for dark matter*, *JHEP* **09** (2016) 018, [[1605.07940](#)].
- [21] M. Cacciari, G. P. Salam and G. Soyez, *The Anti- $k(t)$ jet clustering algorithm*, *JHEP* **04** (2008) 063, [[0802.1189](#)].
- [22] M. Cacciari and G. P. Salam, *Dispelling the N^3 myth for the k_t jet-finder*, *Phys. Lett.* **B641** (2006) 57–61, [[hep-ph/0512210](#)].
- [23] J. Alwall, R. Frederix, S. Frixione, V. Hirschi, F. Maltoni, O. Mattelaer et al., *The automated computation of tree-level and next-to-leading order differential cross sections, and their matching to parton shower simulations*, *JHEP* **07** (2014) 079, [[1405.0301](#)].
- [24] T. Sjostrand, S. Mrenna and P. Z. Skands, *PYTHIA 6.4 Physics and Manual*, *JHEP* **05** (2006) 026, [[hep-ph/0603175](#)].
- [25] T. Sjöstrand, S. Ask, J. R. Christiansen, R. Corke, N. Desai, P. Ilten et al., *An Introduction to PYTHIA 8.2*, *Comput. Phys. Commun.* **191** (2015) 159–177, [[1410.3012](#)].
- [26] DELPHES 3 collaboration, J. de Favereau, C. Delaere, P. Demin, A. Giammanco, V. Lemaître, A. Mertens et al., *DELPHES 3, A modular framework for fast simulation of a generic collider experiment*, *JHEP* **02** (2014) 057, [[1307.6346](#)].
- [27] CMS collaboration, A. M. Sirunyan et al., “Search for narrow and broad dijet resonances in proton-proton collisions at $\sqrt{s} = 13$ TeV and constraints on dark matter mediators and other new particles.” HEPData Repository (based on JHEP 08 (2018) 130), 2018. [[doi:10.17182/hepdata.83912](#)].
- [28] W. Kilian, T. Ohl and J. Reuter, *WHIZARD: Simulating Multi-Particle Processes at LHC and ILC*, *Eur. Phys. J.* **C71** (2011) 1742, [[0708.4233](#)].
- [29] M. Moretti, T. Ohl and J. Reuter, *O’Mega: An Optimizing matrix element generator*, [[hep-ph/0102195](#)].
- [30] S. Baum, R. Catena, J. Conrad, K. Freese and M. B. Krauss, *Determining dark matter properties with a XENONnT/LZ signal and LHC Run 3 monojet searches*, *Phys. Rev.* **D97** (2018) 083002, [[1709.06051](#)].
- [31] A. Buckley, J. Ferrando, S. Lloyd, K. Nordström, B. Page, M. Rüfenacht et al., *LHAPDF6: parton density access in the LHC precision era*, *Eur. Phys. J.* **C75** (2015) 132, [[1412.7420](#)].
- [32] M. Cacciari, G. P. Salam and G. Soyez, *FastJet User Manual*, *Eur. Phys. J.* **C72** (2012) 1896, [[1111.6097](#)].
- [33] R. Brun and F. Rademakers, *ROOT: An object oriented data analysis framework*, *Nucl. Instrum. Meth.* **A389** (1997) 81–86.
- [34] G. Cowan, K. Cranmer, E. Gross and O. Vitells, *Asymptotic formulae for likelihood-based tests of new physics*, *Eur. Phys. J.* **C71** (2011) 1554, [[1007.1727](#)], [Erratum: *Eur. Phys. J.* **C73**,2501(2013)].

- [35] R. Catena, J. Conrad and M. B. Krauss, *Compatibility of a dark matter discovery at XENONnT or LZ with the WIMP thermal production mechanism*, *Phys. Rev.* **D97** (2018) 103002, [[1712.07969](#)].
- [36] CMS collaboration, A. M. Sirunyan et al., *Search for new physics in dijet angular distributions using proton-proton collisions at $\sqrt{s} = 13$ TeV and constraints on dark matter and other models*, *Eur. Phys. J.* **C78** (2018) 789, [[1803.08030](#)].
- [37] CMS collaboration, A. M. Sirunyan et al., *Search for new physics with dijet angular distributions in proton-proton collisions at $\sqrt{s} = 13$ TeV*, *JHEP* **07** (2017) 013, [[1703.09986](#)].
- [38] ATLAS collaboration, G. Aad et al., *Search for New Phenomena in Dijet Angular Distributions in Proton-Proton Collisions at $\sqrt{s} = 8$ TeV Measured with the ATLAS Detector*, *Phys. Rev. Lett.* **114** (2015) 221802, [[1504.00357](#)].
- [39] CMS collaboration, V. Khachatryan et al., *Search for quark contact interactions and extra spatial dimensions using dijet angular distributions in proton-proton collisions at $\sqrt{s} = 8$ TeV*, *Phys. Lett.* **B746** (2015) 79–99, [[1411.2646](#)].